

# AUS Repository

## Experimental Analysis of High Temperature Shape Memory Polymers for Deployable Structures

Item Type	Thesis
Authors	ElMaoud, Mohamad Youssef
Download date	2025-07-03 20:19:25
Link to Item	<a href="http://hdl.handle.net/11073/16480">http://hdl.handle.net/11073/16480</a>

EXPERIMENTAL ANALYSIS OF HIGH TEMPERATURE SHAPE MEMORY  
POLYMERS FOR DEPLOYABLE STRUCTURES

by

Mohamad Youssef ElMaoud

A Thesis presented to the Faculty of the  
American University of Sharjah  
College of Engineering  
In Partial Fulfillment  
of the Requirements  
for the Degree of

Master of Science in  
Mechanical Engineering

Sharjah, United Arab Emirates

June 2019



## Approval Signatures

We, the undersigned, approve the Master's Thesis of Mohamad Youssef ElMaoud

Thesis Title: Experimental Analysis Of High Temperature Shape Memory Polymers For Deployable Structures.

**Signature**

**Date of Signature**

(dd/mm/yyyy)

---

Dr. Wael Abuzaid  
Assistant Professor, Department of Mechanical Engineering  
Thesis Advisor

---

Dr. Maen Alkhader  
Associate Professor, Department of Mechanical Engineering  
Thesis Co-Advisor

---

Dr. Basil Darras  
Associate Professor, Department of Mechanical Engineering  
Thesis Committee Member

---

Dr. Rami Haweeleh  
Professor, Department of Civil Engineering  
Thesis Committee Member

---

Dr. Mamoun Abdel-Hafez  
Head, Department of Mechanical Engineering

---

Dr. Lotfi Romdhane  
Associate Dean for Graduate Affairs and Research  
College of Engineering

---

Dr. Naif Darwish  
Acting Dean, College of Engineering

---

Dr. Mohamed El-Tarhuni  
Vice Provost for Graduate Studies

## **Acknowledgement**

Many thanks to Dr. Wael AbuZaid's direct supervision and support. His direct contribution during the experiments and thorough advice were crucial to the completion of the study.

Moreover, many thanks to my friends and colleagues Mostafa Elyoussef and Mohammad Yousuf for the fruitful technical discussions and lab assistance.

In addition, many thanks to the American University of Sharjah for granting me a Graduate Assistantship for two consecutive semesters, which helped me financially and allowed me to gain useful teaching experience.

The labs of the American University of Sharjah were used throughout the study and the assistance of the lab Technicians Mr. Ronald Almirez and Mr. Dennis Pusing in part of the experiments' preparation was crucial to conducting the needed tests for the study.

## **Dedication**

*To my supportive family, friends, and mentors...*

## Abstract

Shape Memory Polymers (SMP) continue to capture interest of the aerospace industry due to their unique properties. Compared to shape memory alloys, this class of smart materials is lighter in weight and can undergo significantly larger recoverable deformations. However, the recovery stresses, and therefore the loads that can be supported, are inferior compared to shape memory alloys. This limitation has triggered efforts to develop Shape Memory Polymer Composites (SMPC), using SMP epoxy resins, with the ability to overcome the aforementioned drawback. However, the focus has been on SMPs with low transformation temperatures below 100°C. On the other hand, certain aerospace applications require shape memory polymers with higher transformation temperatures to prevent undesirable actuation upon heat exposure. Moreover, and despite significant work on characterizing mechanical and recovery properties of shape memory polymers, the literature lack full field characterization of recovery properties, in particular at elevated temperatures. In this work, a high temperature thermoset epoxy SMP ( $T_g \sim 130^\circ\text{C}$ ), named EPON SMP, is thoroughly investigated. The study provides comprehensive experimental analysis of the mechanical and shape memory properties of the aforementioned high temperature epoxy SMP. In addition, this study uses a full-field characterization technique, Digital Image Correlation (DIC), to provide further insight on localization, heterogeneity and local recovery of shape memory strains. Furthermore, the study evaluates the recovery properties of SMP samples programmed at different loading conditions (*i.e.* bending, tensile) and proposes shape-recovery evaluation methods that can be later implemented on other SMPs. The EPON SMP samples were successfully manufactured and evaluated in this work. Stress free shape recovery was observed for SMP samples programmed at different loading conditions (*i.e.* bending, tensile). Moreover, the recovery rate was found to be dependent on programmed strain level and recovery temperature. Furthermore, the SMP displayed less shape recovery while under stress. Degradation in the SMP's ductility was observed at elevated temperatures. In addition, the effects of thermal stresses and strains were quantified and observed to be highly significant in the SMP programming and shape recovery processes.

**Keywords:** *Shape memory polymer; digital image correlation; shape recovery*

## Table of Contents

Abstract .....	6
List of Figures .....	9
List of Tables .....	11
List of Abbreviations .....	12
Chapter 1. Introduction .....	13
1.1. Overview .....	13
1.2. Thesis Objectives .....	14
1.3. Research Contribution.....	14
1.4. Thesis Organization.....	14
Chapter 2. Background and Literature Review.....	16
2.1. Introduction to SMPs .....	16
2.2. Shape Memory Effect (SME).....	17
2.3. Characterization of SMPs.....	18
2.4. Available commercial SMPs.....	22
2.5. Shape Memory Polymer Composites (SMPCs).....	22
2.6. Possible SMP and SMPC Applications.....	24
2.7. Aerospace Applications.....	25
2.7.1. SMPC hinges.....	26
2.7.2. SMPC booms.....	27
2.7.3. Solar arrays and deployable panels. ....	29
2.7.4. SMPC reflector antennas.....	32
2.8. High temperature SMPs .....	33
Chapter 3. Materials and Methods .....	35
3.1. Samples Preparation .....	35
3.2. Testing for Shape Memory Effect.....	36
3.3. Differential Scanning Calorimetry (DSC) Test.....	37
3.4. Evaluation of SMP Mechanical and Recovery Properties Using Full-Field Characterization Technique (Digital Image Correlation) .....	37
3.4.1. Bending recovery test. ....	38
3.4.2. Temperature dependent mechanical properties. ....	39
3.4.3. Stress relaxation.....	40
3.4.4. Stress-free tensile recovery.....	41
3.4.5. Recovery stress.....	42

3.4.6. Recovery at constant stress.....	44
Chapter 4. Results and Analysis .....	46
4.1. Differential Scanning Calorimetry (DSC) Test.....	46
4.2. Bending Recovery Test .....	46
4.3. Temperature Dependent Mechanical Properties .....	62
4.4. Stress Relaxation.....	64
4.5. Stress-Free Tensile Recovery.....	65
4.6. Recovery Stress .....	68
4.7. Recovery at Constant Stress.....	69
4.8. Recovery Stress - Modified.....	71
Chapter 5. Conclusions and Recommendations.....	73
References.....	75
Vita.....	79

## List of Figures

Figure 1: Conventional dual-shape memory cycle .....	18
Figure 2: Quantitative Thermo Mechanical Analysis (TMA) cycle .....	19
Figure 3: SME stress-strain-temperature relationship .....	19
Figure 4: Polymer network schematic .....	20
Figure 5: Polymer network during shape recovery .....	21
Figure 6: Schematic of structural categorization of SMPs .....	21
Figure 7: Categories of SMPCs .....	23
Figure 8: SMPC hinge .....	26
Figure 9: SMPC hinge during recovery .....	27
Figure 10: Two longeron and three longeron foldable truss booms .....	28
Figure 11: Deployment process of SMPC boom .....	29
Figure 12: Three-longeron boom packaged and deployed configurations .....	29
Figure 13: Coilable SMPC three longeron and six longeron configurations.....	30
Figure 14: STEM boom partially deployed and fully deployed .....	30
Figure 15: Shape memory process of CTD solar array prototype .....	31
Figure 16: CTD solar array design.....	31
Figure 17: RAPDAR concept .....	32
Figure 18: Solid surface reflector developed by CTD .....	33
Figure 19: Deployment stages of antenna.....	33
Figure 20: Sample preparation.....	36
Figure 21: Programming and recovery process of SMP .....	37
Figure 22: Experimental setup .....	38
Figure 23: Different geometry samples .....	39
Figure 24: Bending recovery test samples preparation.....	40
Figure 25: Tensile test sample .....	41
Figure 26: Stress relaxation method .....	41
Figure 27: Recovery stress initial method .....	43
Figure 28: Recovery stress method - modified .....	44
Figure 29: Recovery at constant stress method.....	45
Figure 30: DSC test result - EPON SMP.....	47
Figure 31: EPON recovery.....	47
Figure 32: Analyzed regions .....	48

Figure 33: EPON sample horizontal displacement vs. time .....	49
Figure 34: Horizontal displacement ( $U$ ) validation .....	50
Figure 35: EPON sample vertical displacement vs. time .....	51
Figure 36: Vertical displacement ( $V$ ) validation .....	52
Figure 37: EPON sample von-mises strain vs. time .....	52
Figure 38: EPON sample in-plane rotation angle vs. time .....	54
Figure 39: Rotation angle validation.....	55
Figure 40: EPON samples comparison - horizontal displacement rate .....	56
Figure 41: EPON samples comparison - vertical displacement rate.....	57
Figure 42: EPON samples comparison – von-mises strain rate.....	57
Figure 43: EPON samples comparison - time to 100% recovery .....	57
Figure 44: Different bending angles comparison - horizontal displacement.....	58
Figure 45: Different bending angles comparison - vertical displacement .....	58
Figure 46: Different bending angles comparison - von-mises strain.....	59
Figure 47: Different bending radii comparison - horizontal displacement.....	59
Figure 48: Different bending radii comparison - vertical displacement .....	60
Figure 49: Different bending radii comparison - von-mises strain.....	60
Figure 50: Different oven temperature comparison - horizontal displacement .....	61
Figure 51: Different oven temperature comparison - vertical displacement .....	61
Figure 52: Different oven temperature comparison - von-mises strain .....	62
Figure 53: Tensile test of EPON SMP at different temperatures.....	63
Figure 54: Poisson ratio at multiple temperatures .....	64
Figure 55: EPON SMP stress relaxation at different temperatures .....	65
Figure 56: Normalized stress relaxation after loading .....	66
Figure 57: Normalized stress relaxation after returning to initial position.....	67
Figure 58: Stress-free thermal expansion .....	67
Figure 59: Stress-free tensile recovery .....	68
Figure 60: Recovery stress initial results .....	69
Figure 61: Recovery at constant stress 2 MPa .....	70
Figure 62: Recovery at constant stress 0.5 MPa.....	70
Figure 63: Recovery at constant stress 1 MPa.....	71
Figure 64: Recovery stress – modified .....	72

## **List of Tables**

Table 1: Comparison of properties of Ti/Ni SMA with a typical SMP.....	17
Table 2: Possible SMP applications.....	25
Table 3: Tensile test summary .....	64
Table 4: Recovery at constant stress summary .....	72

## **List of Abbreviations**

ASTM	American Society for Testing and Materials
DIC	Digital Image Correlation
DMA	Dynamic Mechanical Analysis
DSC	Differential Scanning Calorimetry
MSMP	Multiple Shape Memory Polymer
RT	Room Temperature
SMA	Shape Memory Alloy
SMC	Shape Memory Ceramic
SME	Shape Memory Effect
SMP	Shape Memory Polymer
SMPC	Shape Memory Polymer Composite
TMA	Thermo-Mechanical Analysis
UTM	Universal Testing Machine

## Chapter 1. Introduction

In this chapter, the potential of Shape Memory Polymers (SMPs) and their limitations in aerospace applications are introduced. The motivation and the objectives for this research are discussed. Moreover, the contributions of this research are listed, and the general organization of this thesis report is then presented.

### 1.1. Overview

Recent advances in SMPs have highlighted the high potential for their use as actuators in aerospace applications. SMPs can be programmed into a temporary shape, then return to the permanent shape (*i.e.*, original synthesized shape) with exposure to a specific external stimulus. In addition, SMPs are light-weight, can undergo high recoverable deformations ( $> 100\%$ ) and can be easily fabricated into a wide range of structural designs [1]. However, the applications are limited mainly due to their low recovery stresses, therefore low load carrying capacity, and low transformation temperatures. Furthermore, SMPs have relatively inferior functional fatigue life and exhibit slower response/actuation times compared to Shape Memory Alloys (SMAs). Such limitations can cause incomplete and/or uncontrollable deployment which leaves the reliability of using SMPs in aerospace applications questionable. Therefore, researchers have been motivated to further study and develop SMPs in order to utilize their high potential in aerospace applications while overcoming their limitations.

To address one of the major limitations of SMP, *i.e.*, their low stiffness and strength, research efforts have been focused on developing Shape Memory Polymer Composites (SMPCs) with enhanced mechanical properties. These development efforts aim to produce SMPCs with similar behavior to traditional aeronautics grade epoxy matrix composites [2]. However, the current focus has been on the use of SMPs with low transformation temperatures below  $100^{\circ}\text{C}$  [3,4]. Studies show that most thermally responsive shape memory epoxies have glass transition temperatures ranging between  $44\text{-}98^{\circ}\text{C}$  [5,6,7]. On the other hand, the glass transition temperatures for aeronautics grade epoxy matrix composites, with no shape memory properties, are observed in the range of  $100\text{-}200^{\circ}\text{C}$  [4]. Therefore, a high temperature SMP is needed as a matrix for aeronautics grade SMPCs. Researchers from NASA Glenn Research Center developed a thermally responsive thermoset Epoxy SMP with a transformation temperature higher than  $130^{\circ}\text{C}$  [5]. Yet, there is little analysis of the recovery properties of this SMP. In

addition, and despite significant work on characterizing mechanical and recovery properties of SMPs, current studies lack full-field characterization, in particular focusing on the local recovery properties.

## **1.2. Thesis Objectives**

Driven by the interest of expanding the range of use of SMPs in aerospace applications, a high temperature thermoset epoxy SMP is investigated in this research. Moreover, driven by the interest of understanding SMPs' potential in aerospace applications, a series of mechanical and unique recovery tests are conducted on this SMP. Furthermore, evaluation of the results is conducted using Digital Image Correlation (DIC) technique in order to quantify the mechanical and recovery properties of the SMP in local regions of the material. Through the use of full-field analysis (DIC), further insight into the localization, heterogeneity, and local recovery of shape memory strains is provided. The objectives of this research are as follows:

- To study the mechanical and recovery properties of a high temperature epoxy SMP which can be later used as an epoxy matrix for possible high temperature SMPCs.
- To provide full-field characterization of the mechanical and recovery properties of SMPs where the used methods can be later used to evaluate other SMPs.

## **1.3. Research Contribution**

The contributions of this research work can be summarized as follows:

- Provide comprehensive experimental analysis of the mechanical and shape memory properties of an advanced high temperature epoxy shape memory polymer for aerospace applications. This epoxy SMP can be used as a matrix for aerospace grade SMPCs.
- Study the global and local shape recovery properties under uniform (tension) and non-uniform deformation (bending) programmed shapes.
- Propose shape-recovery evaluation methods which can be repeated for evaluation of other SMPs/SMPCs.

## **1.4. Thesis Organization**

The rest of this thesis is organized as follows: Chapter 2 provides background on SMPs, SMPCs and their aerospace applications. Moreover, related works on

evaluation of mechanical and recovery properties of SMPs are discussed. The materials and methods used are discussed in chapter 3. Chapter 4 provides the extracted results along with their analysis. Finally, Chapter 5 concludes the thesis and outlines the proposed future work.

## Chapter 2. Background and Literature Review

In this chapter, an introduction on SMPs and description of the Shape Memory Effect (SME) are provided. Moreover, the characterization of SMPs is discussed. In addition, there is an overview on the currently available commercial SMPs. SMPCs are then discussed and the possible SMP/SMPC applications are introduced. Finally, a summary of the available aerospace applications is provided.

### 2.1. Introduction to SMPs

Smart materials are defined as materials that can sense the environment and/or their own state, make a judgment and then change their functions according to a predetermined purpose [9]. Smart functions provided by smart materials are intrinsic properties of the material and are different from smart systems or facilities that rely on complicated sense-response structure of feedback systems. Such intrinsic senses are environmentally related such as sensing the change of temperature, electric current, magnetic flux, PH values, optical wavelength, etc. Shape Memory Materials (SMMs) are a type of smart materials that can be programmed into a temporary shape, then return to their permanent shape (*i.e.*, original synthesized shape) with exposure to external stimulus. SMMs are mainly divided into Shape Memory Alloys (SMAs), Shape Memory Polymers (SMPs) and Shape Memory Ceramics (SMCs). Research on this type of materials has been attracting significant interest due to the wide range of potential applications for this class of materials.

SMPs were not recognized until the 1960s when heat shrinkable tubes and films were made using crosslinked polyethylene. Efforts were made to develop SMPs in the 1980s and 1990s but no significant progress was made until the past decade. During this period, SMPs were investigated thoroughly and several advantages were noticed. To begin with, SMPs can use diverse external stimulus and triggers that can even co-exist making the material multi-sensitive. In addition, they show high flexibility in programming making them suitable for a wide and diverse range of applications. Moreover, they can be fabricated into a wide range of permanent shapes and structural designs. Also, they possess tunable properties that can be easily engineered and tuned using composites, blending and synthesis. Furthermore, some SMPs are soft and biodegradable making them suitable for medical applications. In addition, they are very

light and can occupy large volumes when made into foams which makes them suitable for aerospace applications. Finally, they are considered to have low cost when compared to SMAs. Despite the numerous advantages, SMPs have some major drawbacks such as having low stiffness that results in low recovery stress compared to SMAs. Moreover, they show long response time until shape recovery. Also, under cyclic loading conditions, SMPs have been shown to exhibit lower lives and relatively inferior cyclic stability compared to SMAs. Table 1 compares the properties of a typical SMP with Ti/Ni SMA to clearly identify some of the advantages and disadvantages [9].

Table 1: Comparison of properties of Ti/Ni SMA with a typical SMP [9]

MATERIAL/PROPERTY	TI/NI SHAPE MEMORY ALLOY	SHAPE MEMORY POLYMER
Recovery Stress	200-400 MPa	1-3 MPa
Recovery strain	6%	50-600%
At low temperature	Soft ( $E_s$ )	Hard ( $E_s=100E_h$ )
At high temperature	Hard ( $E_h = 2E_s$ )	Soft ( $E_h$ )
Density	6-7 g/cm <sup>3</sup>	1 g/cm <sup>3</sup>
Phase transformations	Martensitic, R-phase	Glass Transition
Shaping	Difficult	Easy
Cost	Expensive	Cheap
Heat conductivity	High	Low

## 2.2. Shape Memory Effect (SME)

Polymer SME can be triggered using various stimuli as mentioned before but thermal stimulus is the conventional one. The most basic form of polymer SME is shown in Figure 1 while Figure 2 shows its quantitative thermomechanical analysis cycle [10]. To begin with, the SMP is heated above its reversible thermal transition temperature (*i.e.* glass transition temperature ( $T_g$ ) or melting temperature ( $T_m$ )) where the SMP transitions to its soft phase. Then, the SMP will be loaded and deformed then cooled down under its thermal transition temperature while maintaining the

deformation. After the load is removed, a temporary shape will be fixed (*i.e.* Shape fixing). Finally, shape recovery to the SMP's permanent shape (*i.e.* synthesized shape) will occur by stress-free heating above the SMP's thermal transition temperature. Figure 3 shows a plot of the shape memory cycle involving stress, strain, and temperature [2,11]. The ability of the SMP to fix and recover shapes is respectively defined as shape fixity ( $R_f$ ) and shape recovery ( $R_r$ ) such that:

$$R_f = \frac{\varepsilon}{\varepsilon_{load}} * 100\% \quad (1)$$

$$R_r = \frac{\varepsilon - \varepsilon_{rec}}{\varepsilon} * 100\% \quad (2)$$

where  $\varepsilon_{load}$  is the maximum strain under load,  $\varepsilon$  is the fixed strain after cooling and load removal, and  $\varepsilon_{rec}$  is the strain after recovery. SMPs can be evaluated by the strain recovery rate or also called recovery speed which is the time derivative of strain as shown below:

$$V_r = \frac{\partial \varepsilon}{\partial t} * 100\% \quad (3)$$

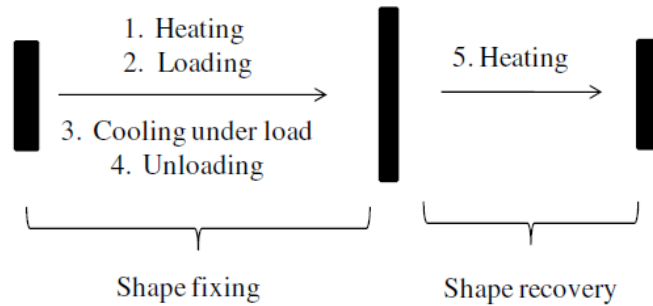


Figure 1: Conventional dual-shape memory cycle [10]

### 2.3. Characterization of SMPs

SMPs possess three-dimensional molecular network-like architectures that are thought to be constructed through crosslinking net points with polymer segments connecting them. Those net points can be either physically crosslinked or chemically crosslinked structures. Physically crosslinked polymers are thermoplastics which means they exhibit a reversible nature. Furthermore, physically crosslinked networks are achieved by the formation of crystalline or glassy phases between the polymer chains. On the other hand, chemically crosslinked polymers are thermosets which

means they exhibit an irreversible nature. The interconnection between polymer chains in chemically crosslinked networks is achieved by covalent bonds which are more stable than the physical crosslinks. The physical and chemical crosslinks are illustrated in Figure 4.

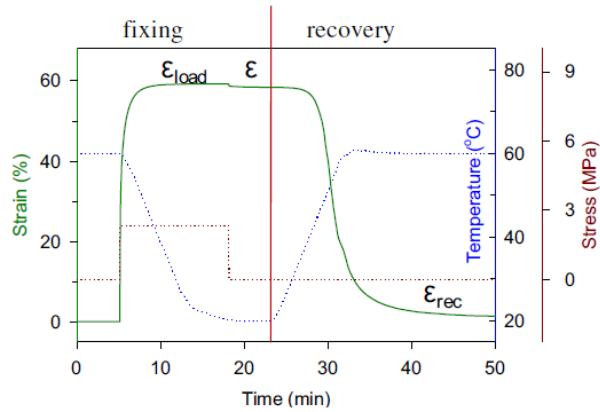


Figure 2: Quantitative Thermo Mechanical Analysis (TMA) cycle [10]

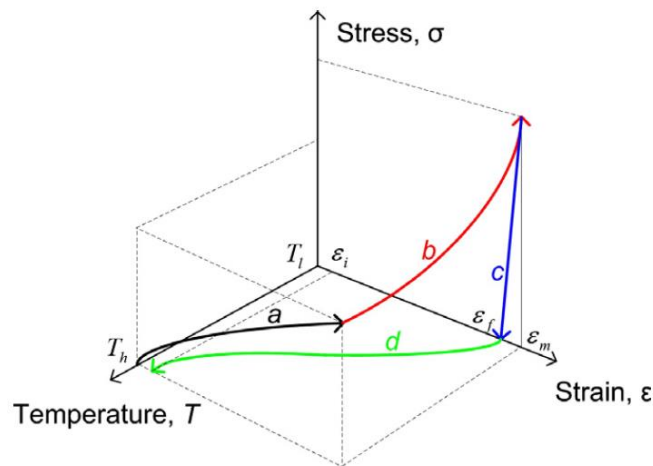


Figure 3: SME stress-strain-temperature relationship [2,11]

It is essential for the SMP to form secondary crosslinks which are strong reversible interactions between the polymer segments. This allows for a temporary shape deformation to be fixed. Once the SMP is heated above its transition temperature, the polymer chains are randomly coiled between the net points. After applying a stretching stress, polymer segments will be elongated but still coiled. After cooling while maintaining the deformed shape, secondary crosslinks will be formed on the

elongated segments as shown in Figure 5. These secondary crosslinks can be of either glassy or crystalline phases. In addition, the transition temperature of SMP's can be either a glass transition temperature ( $T_g$ ) or melting temperature ( $T_m$ ). Finally, after reheating above the transition temperature, the secondary crosslinks will detach for the shape memory effect to occur. The strain energy will be released causing the occurrence of the SMP recovery process.

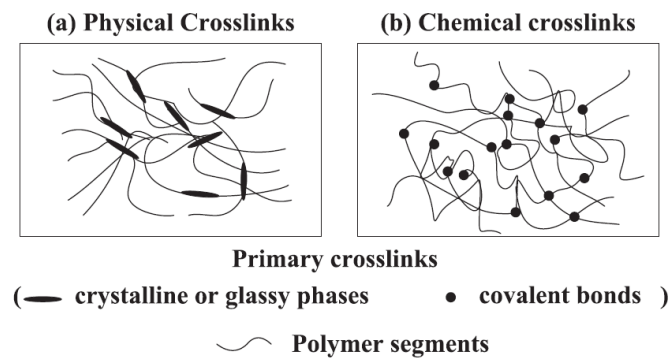


Figure 4: Polymer network schematic [12]

As mentioned earlier, SMPs can be either physically crosslinked or chemically crosslinked. These materials are usually classified based on the type of crosslinking and the transition temperature needed to activate the SME. Firstly, we have physically crosslinked thermoplastics with a transition temperature  $T_g$ . Secondly, physically crosslinked thermoplastics with a transition temperature  $T_m$ . Thirdly, chemically crosslinked amorphous polymers with a transition temperature  $T_g$ . Lastly, we have chemically crosslinked semi-crystalline polymer networks with a transition temperature  $T_m$ . Thermoplastic SMPs exhibit relatively poor thermal and mechanical properties when compared to thermosets which are styrene or epoxy based SMPs. Thermosets have higher shape recovery ratio, better elastic modulus at room temperature and better stability against moisture or space radiations. Those differences are the reason why thermoplastics such as polyurethane SMP's are mostly researched to be used as functional materials such as biomaterials and SMP textiles. On the other hand, styrene-based and epoxy-based SMPs are used as structural materials such as mobile actuators or aerospace deployable structures. Figure 6 [13] shows a schematic of structural categorization of SMPs based on their crosslinking.

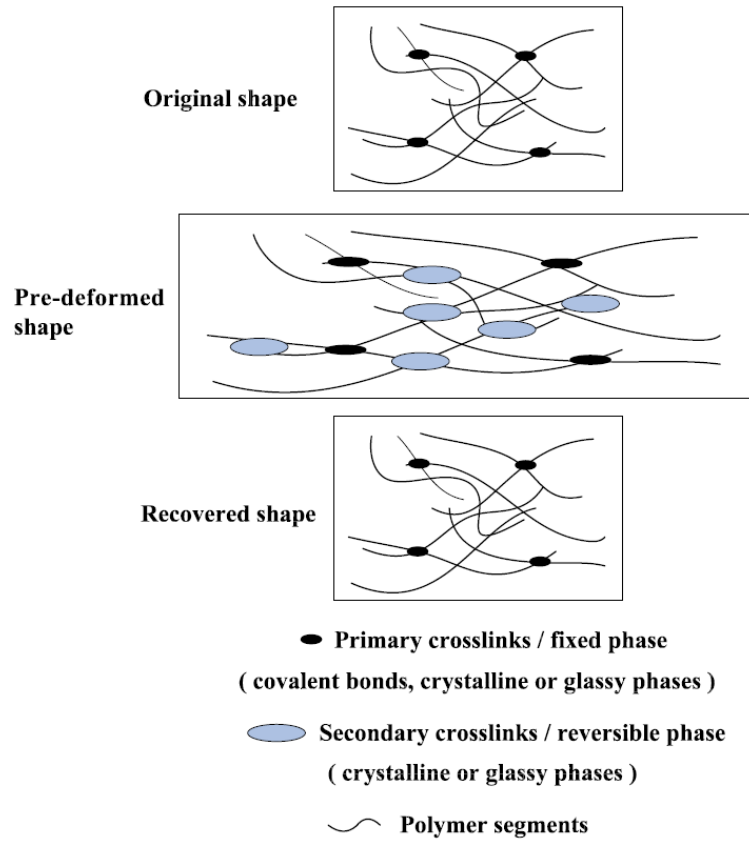


Figure 5: Polymer network during shape recovery [14]

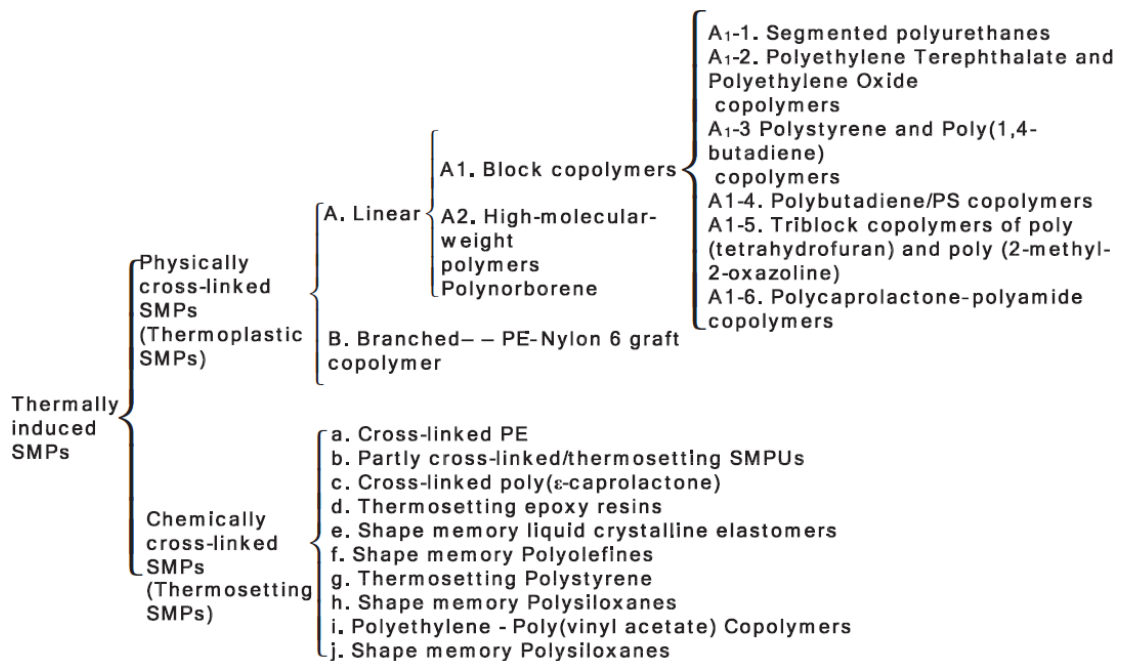


Figure 6: Schematic of structural categorization of SMPs [13]

#### **2.4. Available Commercial SMPs**

Many commercial and non-commercial SMPs are reported in the literature. As for commercially available SMPs, Mitsubishi Heavy Industries produce one of the most widely known commercially available SMPs which are thermoplastic polyurethanes. In addition, Cornerstone Research Group (CRG) produce the two-part styrene based thermoset SMP resin that goes with the trade name “Veriflex”. Moreover, Composite Technology Development (CTD) produce the commercially available TEMBO family of epoxy based SMPs such as TEMBO 3XE. Furthermore, the one-part heat curable epoxy resin Scotchkote 206N is made by 3M. Also, Polymer Technology Group in Berkeley produce the Porous Calomer 48 SMP. Ranwal Ltd produce an SMP foam under the trade name of FLEGMAT. In addition, Lubrizol Advanced Materials produce Tecoflex which is a medical grade polyurethane used in a wide range of medical implants. Finally, an Ultraviolet curable Polyurethane NOA-63 is produced by Norland Products Incorporation [15].

#### **2.5. Shape Memory Polymer Composites (SMPCs)**

As mentioned earlier, SMPs have the advantage of being light weight, low cost, good process-ability, high recovery strain, and highly flexible programming when compare to SMAs. On the other hand, SMPs intrinsically have low mechanical strength and low recovery stresses which limit its possible applications. To address these limitations, some research efforts have been dedicated to explore improving the strength and load carrying capacity of SMPs through the synthesis of shape memory polymer composites (SMPC). SMPCs can reinforce the polymer mechanical properties, enhance athermal stimuli active effects, introduce novel shape memory effects and allow for new functions. Different types of SMPCs have been achieved through different blends and fillers, as shown in Figure 7, are introduced in this chapter of the report [8].

SMPCs are used to reinforce the mechanical properties of the SMP through physical blending, in-situ polymerization and through chemical crosslinking. Firstly, SMPs can be reinforced with microfibers or fabrics such as carbon fibers, glass fibers, and Kevlar fibers. This reinforcement results in remarkably increasing the mechanical strength of SMPs. This type of composites can withstand higher load in the fiber direction while barely maintaining the SME in the transverse direction. Such reinforced

SMPCs are used for spacecraft deployable structures (Elastic Memory Composites), and vibration control structures. Secondly, SMPs are can be blended with carbon nanotubes (CNT) or carbon nanofibers (CNF) which improves the mechanical strength and shape recovery stress of the SMP. Moreover, CNTs and CNFs give the SMP potential electrical and infrared-light-active shape memory effect. Thirdly, organic exfoliated Nano-clay is used to prepare functional composites with advanced properties. Recent research is being done in order to enable the Nano-clay’s reaction with the SMP matrix. Fourthly, Silicon Carbide (SiC) and Silicon Dioxide (SiO<sub>2</sub>) are also used as fillers to SMPs. SiO<sub>2</sub> proved to be a better filler than SiC since SiC deteriorates the SME of SMPs even at low temperatures. The fifth filler reported in the literature is conducting Carbon Black (CB) which enhances the electrical conductivity of SMPs while severely deteriorating the shape recovery process. Lastly, other organic and inorganic fillers are used providing a wider range of possible properties of SMPCs. An example to organic fillers is cellulose nanoparticles while Celite is an example for inorganic fillers used.

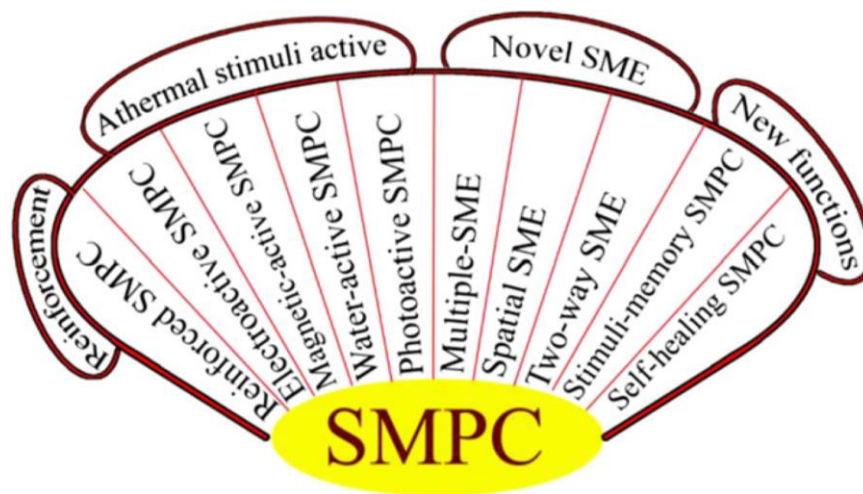


Figure 7: Categories of SMPCs [8]

Due to the wide range of fillers and blends used on SMPCs, different athermal stimuli-active effects are achieved. To begin with, electroactive SMPCs with improved electrical conductivity are made by filling the SMPs with enough electrical conductive particles such as CB, CNT and CNF. Furthermore, magnetic active SMPCs with

improved magnetic properties are suitable for medical applications and are achieved by incorporating magnetic particles. Such magnetic particles can be metal particles, ferromagnetic particles, nickel powders, or iron (III) Oxide particles, etc. In addition, water active SMPCs are also reported in the literature and are achieved by filling the SMP with a hydrophilic ingredient or by cellulose Nano-whiskers. Finally, photoactive or light active SMPCs have been developed and are based on different fillers and blends. Further research is in progress in order to improve the properties and obtain new functions of these SMPCs.

To conclude this chapter, the different novel shape memory effects and new functions realized by SMPCs are discussed. Multiple SME have been developed to cover a wider range of applications. MSMP can remember more than one temporary shape while still remembering the original permanent shape through multiple step programming. This is significant in the field of packaging and robotics. Moreover, spatially controlled SMPCs are developed by utilizing the thermal insulation property of the polymer. Since polymers are good insulators, it is possible to apply heat locally while not thermally affecting the whole structure. This allows for spatially controlling the recovery process by triggering it in specific locations of the structure only. Furthermore, two-way SMPCs are developed where heating and cooling changes the shapes of SMPs reversibly. Moreover, new functions such as stimuli memory effect of SMPCs are being reported in the literature. Stimuli memory effect means that the material remembers the value of the stimuli parameter being applied when they are deformed. Temperature memory effect and magnetic memory effect of SMPCs are reported in the literature. Further research in this function allows for linking stimuli parameters with recovery aspects of the SMPs and have potential in sensors applications. Finally, SMPCs are developed in self-healing applications where they utilize the intrinsic healing capability of SMPs in order to repair macroscopic cracks. The self-healing capability allows for a wide range of applications such as self-repairing aerospace structures.

## **2.6. Possible SMP and SMPC Applications**

SMPs are considered a novel type of smart materials that are used for a wide range of applications in different fields. These materials are used in the areas of biomedicine, smart textiles, self-healing composites, automobile actuators and

aerospace. Table 2 shows a list of various developed SMP applications that are found in the literature [8].

Table 2: Possible SMP applications [8]

Applications		Applications	
1	Aneurysm occlusion devices	34	Orthodontic
2	Assembly/disassembly tools	35	Orthopedic cast
3	Bio-MEMs	36	Orthopedics Morphix® suture anchor
4	Bone defect fillers	37	Packaging
5	Cardiac valve repair	38	Pharyngeal mucosa reconstruction
6	Cells manipulating and capturing	39	Phase change fabrics
7	Chemical feeding in chemical reactions	40	Physiological monitoring
8	Clot removal devices	41	Post-surgical treatment of mitral insufficiency
9	Controlled drug release	42	Pressure garments
10	Crease and pattern retention finishing	43	Recordable and erasable memories
11	Damping fabrics	44	Study of cell proliferation
12	Damping materials	45	Selective desalination material
13	Deodorant fabrics	46	Self-healing
14	Electroactive shape memory hinge	47	Self-peeling dry adhesive
15	Embolic devices	48	Shape changing nanofibers
16	Endoscopic surgery suture	49	Shape memory fibers
17	Erasable Braille	50	Smart mandrels for composite tooling
18	Fashion design	51	Shape memory neuronal probe
19	Flexible light-emitting diodes	52	Skin-care products
20	Hair treatment	53	Soft lithography
21	Heat and moisture management	54	Surface wetting
22	Heat shrinkable packages for electronics	55	Microfluidic devices
23	Hot shrinkage micro-tags	56	Surface wrinkle and micro-patterns
24	Kidney dialysis needles	57	Switchable information carriers
25	Light-modulators and display devices	58	Temperature sensors
26	Measuring tools in complex cavities	59	Toys
27	Memory foam mattress, pillow and insoles	60	Treatment of esophageal stenosis
28	MEMs applications	61	Vascular stents
29	Microtweezers in medicine	62	Surgery inside living cells
30	Micro-valves in microdevices	63	Vehicle active air dams and other aerodynamic surfaces
31	Morphing of aircraft wings and helicopter rotor blades	64	Weight reducing agent
32	Novel McKibben artificial muscles	65	Wound dressing
33	Ophthalmic applications	66	Wrinkle free finishing of cotton fabrics

## 2.7. Aerospace Applications

In aerospace applications, the use of such materials in large area antennae and solar cell arrays is attractive because the materials can be stored in low volume and then self-deployed while in space [16, 3]. SMPs/SMPCs are believed to be well-suited to create a shape-memory effect in some aircraft structures. SMPs/SMPCs are lightweight, can achieve high strain rates, and can be tailored to display high strength and thermal properties [17, 18]. A very similar behavior to traditional aeronautics grade epoxy matrix composites can be achieved by using shape memory epoxies in making SMPCs [5].

Nowadays, much research is devoted to applications of SMP/SMPC in the aerospace field. Shape memory materials currently cover a wide range of aerospace applications including hinges, trusses, booms, antennas, optical reflectors, and morphing skins. However, space environment is extremely harsh, and many important factors should be considered when selecting structure materials for such an environment. Those factors include high vacuum, ultra-high or low temperature cycle effect, ultraviolet (UV) radiation, etc. Necessary testing should be done before applying SMPs in the space-deployable structures. Since traditional aerospace structures are intrinsically high weight, high cost, and have high deployable shock effect, the need of more effective materials is needed and SMPs will be one of the best candidates for such materials. This chapter will list the different types of structures currently developed in the aerospace field.

**2.7.1. SMPC hinges.** A hinge can usually be the driving device in the deployment process of space deployable structures. There are many important factors to rate its effectiveness such as shock effect and recovery precision. Traditionally, mechanical hinges or tape spring hinges were used for the deployment process. Due to the complex integrated system of the mechanical hinge and the large shock effect of the spring steel hinge, the challenge of successful deployment increased. Therefore, CTD introduced a new type of hinge composed of Elastic Memory Composite (EMC) materials to reduce moving parts and the shock effect. Testing results showed that this hinge can provide good controllable deployment ability.



Figure 8: SMPC hinge [19]

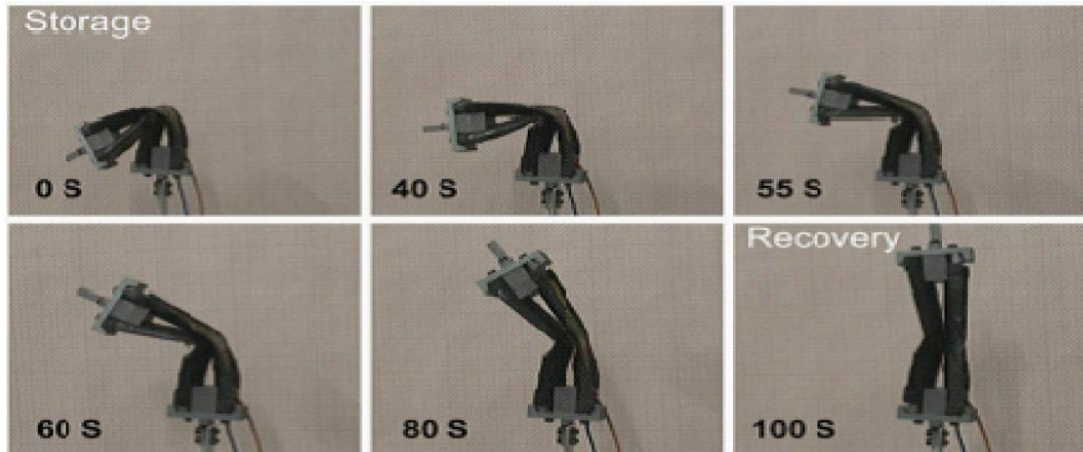


Figure 9: SMPC hinge during recovery [20]

**2.7.2. SMPC booms.** Booms are the main components to support the tip payloads in satellites. The design of space deployable boom mostly used metals and involved complex assembly and control mechanisms resulting in an overall high weight. Research is being done on different methods to overcome this problem and currently SMPC booms are being developed. SMPC space deployable booms have a simpler structure than the traditional ones. Moreover, it packages and deploys without the need of mechanical devices. Novel types of space deployable booms are divided into foldable SMPC truss booms, coilable SMPC truss booms, and storable tubular extendible member SMPC booms.

**2.7.2.1. SMPC foldable truss booms.** As for the foldable truss booms, CTD developed a new type of EMC space deployable booms under the funding United States Air Force Academy's (USAFA) Air Force Research Laboratory (APRL). Two types of boom configurations, shown in Figure 10, were chosen as the best candidates for the FalconSat-3 mission. The one on the left is a three longeron truss boom which will be extensible to a space triangle shaped truss boom. The other one on the right is a two-longeron truss boom that will form a tubular shaped boom after deployment. Starsys Research Company (SRC) studied the feasibility of EMC truss booms and selected the best structure. It was indicated that the moving of the two-longeron boom and the fastening of the three longeron boom are potential failure factors to successful deployment. After the evaluation, the low moving part and light weight design of the three longeron boom led to its selection as the preliminary baseline model for the

FalcoSat-3 mission. Figure 12 shows the selected design's packaged and deployed configurations. In addition, Figure 11 clearly shows the deployment process of the SMPC boom.

**2.7.2.2. SMPC coilable truss booms.** Coilable SMPC booms is another advanced type of space deployable booms being developed. It consists of a simple light weight structure however high strain energy and large relaxation phenomena exist in the stowed state. Currently, there are three longeron and six longeron truss boom configurations. The longeron can be bent or stowed in a small volume to provide stiffness and strength after deployment. Deployment of these booms can be free deployment, cable deployment, or tubular deployment. As for the three longeron coilable truss boom, it is a free deployment boom basically composed of longeron, lateral batten, and diagonal members as shown in Figure 13 (left). S2-glass/epoxy is used to fabricate the longeron however it is a safety challenge since the boom will store lots of strain energy when packaged and twisting it to helical shape for launch. Therefore, fiber-reinforced composite is used to fabricate the longeron and it proved to significantly reduce the weight and packaged strain energy while maintaining high strain capability.

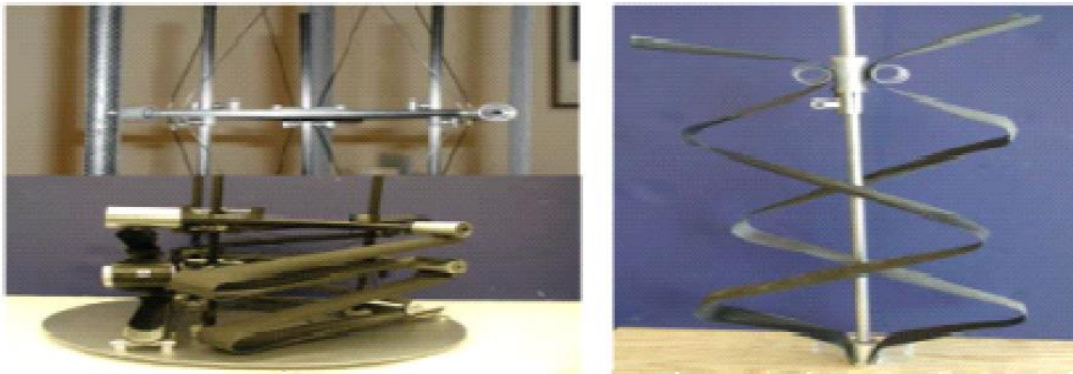


Figure 10: Two longeron and three longeron foldable truss booms [21]

**2.7.2.3. SMPC storable tubular extendible member booms.** Storable Tubular Extendible Member (STEM) SMPC booms have lower weight, higher packaging strain, and stronger specific modulus than the traditional STEM booms. In addition, STEM has a simpler structure and larger cross-section compared to conventional SMPC

booms. A seven meters horizontal SMPC STEM boom is shown in Figure 14 where it is partially deployed on the left photo and fully deployed in the right one.

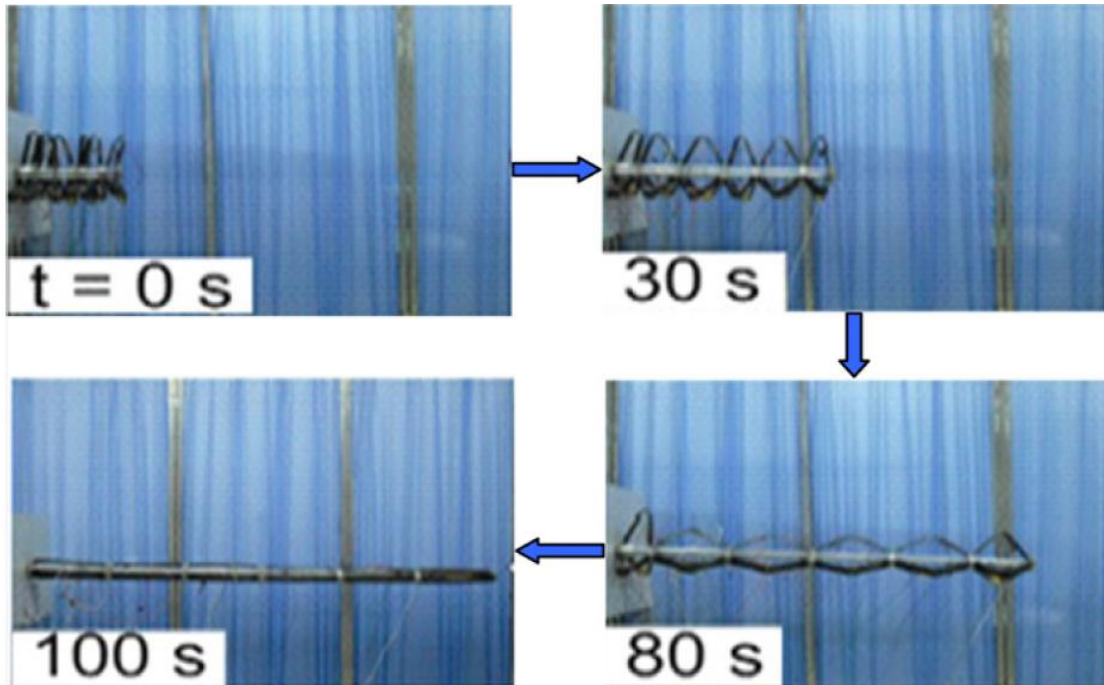


Figure 11: Deployment process of SMPC boom [22]

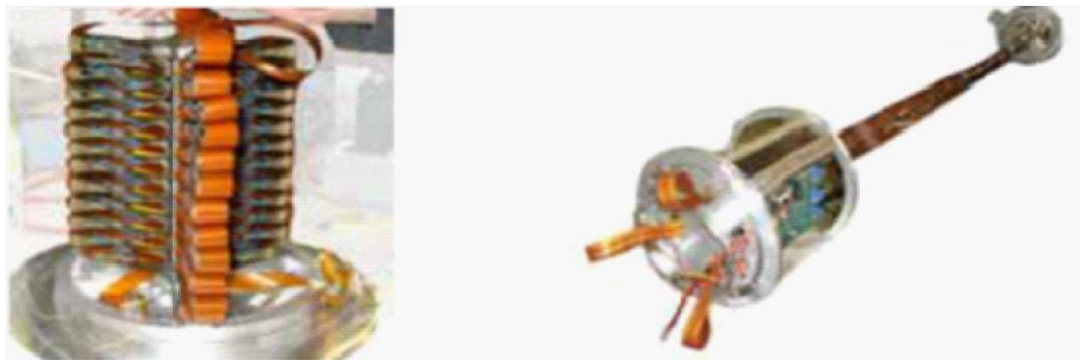


Figure 12: Three-longeron boom packaged and deployed configurations [22]

**2.7.3. Solar arrays and deployable panels.** Solar arrays are the main energy generation systems in space deployable structures and are commonly packaged in the space vehicles before launch. It is deployed while the space vehicle is orbiting in order to collect solar energy needed for the space-structure functioning. The efficiency of

these solar arrays depends on large deployment areas, reliable stiffness and lightweight. These structures can vary in flexibility from highly rigid to highly flexible structures. Researchers have developed a carbon fiber reinforced SMPC hinge to actuate the solar deployment and simulated the deployment process in zero-gravity environment as shown in Figure 15.

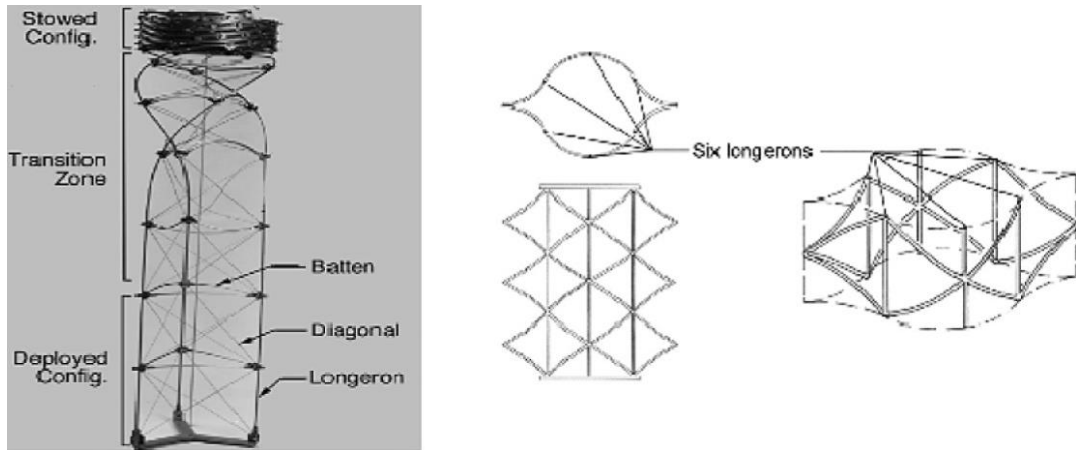


Figure 13: Coailable SMPC three longeron and six longeron configurations [23]



Figure 14: STEM boom partially deployed and fully deployed [24]

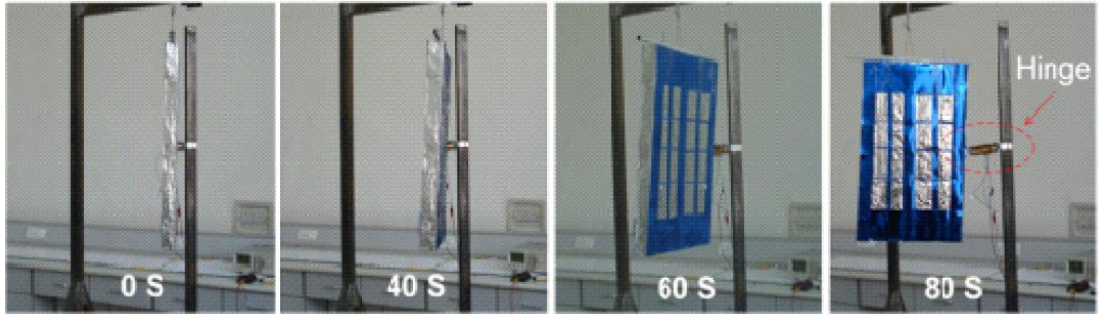


Figure 15: Shape memory process of CTD solar array prototype [20]

Moreover, CTD developed a type of solar array, shown in Figure 16, with low moving parts, simple structure and low cost. This solar array's mission is to advance the operationally responsive space technology and validate the advantages of the new design to better adapt to different types of missions for future small satellites. The key factor to achieve this is the use of EMC hinges. These EMC hinges are designed to deploy the solar array and then damp the deployment to lock it to a certain desired position as shown in Figure 16.

Since the design and architecture of solar arrays are important factors to improve the efficiency of collecting energy, another kind of deployable solar arrays are developed by CTD. The Roll-out And Passively Deployed Solar Array (RAPDAR) consists of two EMC booms and several pieces of thin –film photovoltaic solar arrays where the EMC booms activate the solar array deployment process, shown in Figure 17, and support the array. RAPDAR requires larger deployable areas to provide enough energy for the satellites.

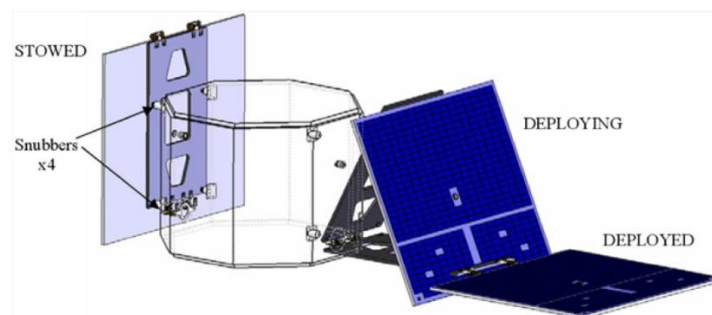


Figure 16: CTD solar array design [25]

**2.7.4. SMPC reflector antennas.** The antenna is the important communication tool between the satellites and the earth while in space. Two main parameters measure the antenna's working properties which are the reflector aperture and precision however these properties can be contradictory in some ways. If these two properties are satisfied simultaneously, the structure will be too complex. Different structure models are proposed such as the wrap-rib deployable antenna, rigid-rib deployable antenna, the hinged-rib deployable antenna and the tension truss antenna. All these antennas have major drawbacks where SMPCs can be used to overcome them.

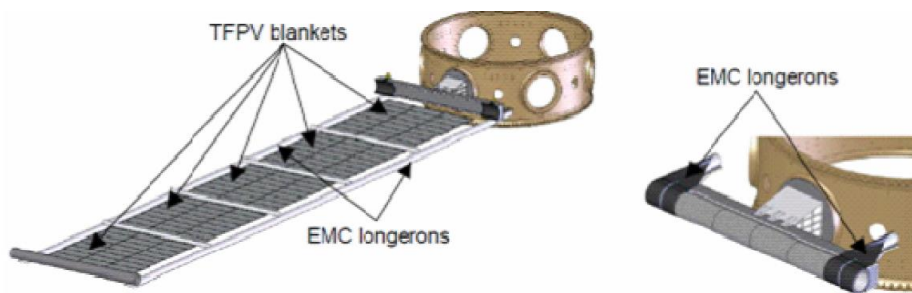


Figure 17: RAPDAR concept [26]

CTD developed a high frequency solid surface deployable reflector to better meet the requirements of future satellite missions in aerospace engineering. These reflectors include furlable graphite composite membrane, support struts and EMC outer stiffener as shown in Figure 18. The EMC stiffener is the key element to element on the reflector since it provides the deployment force for the reflector and become the important supporting structure after deployment. Testing shows the EMC stiffener with high strain capability can be packaged into the stowed configuration under high temperature and return to the deployed shape without large shock effect, when reheated above the EMC transition temperature.

In addition, Harris company considered using the concept of SMPCs to design a new type of smart solid surface deployable reflectors called the Flexible Precision Reflector (FPR) and created some models for the deployment experiment as shown in Figure 19. This model consists of two parts: the outer stiffener fabricated using an EMC material and a thin film surface reflector in the middle part.

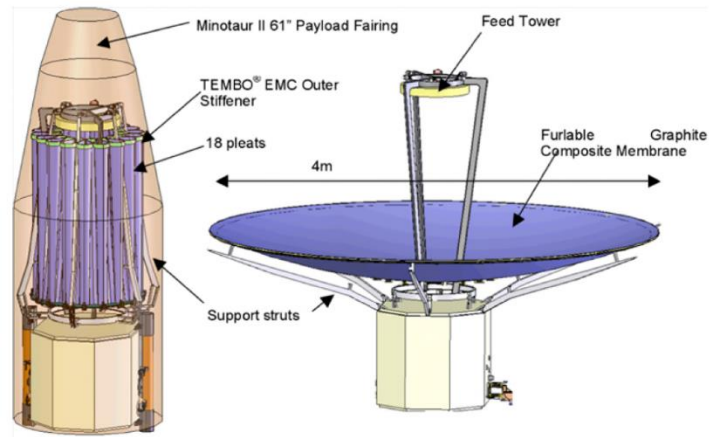


Figure 18: Solid surface reflector developed by CTD [27]

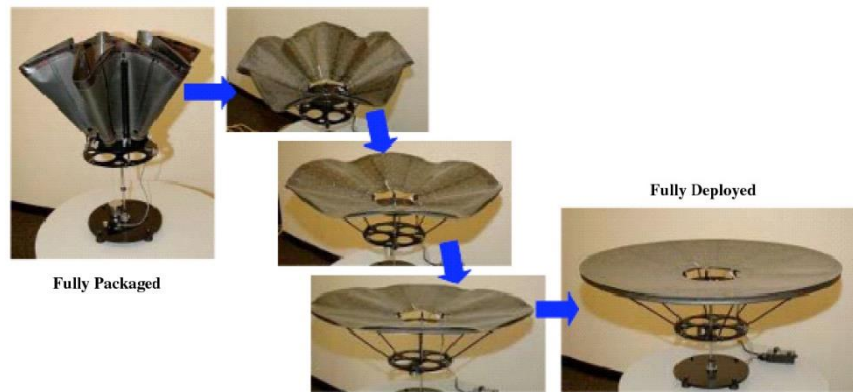


Figure 19: Deployment stages of antenna [28]

## 2.8. High temperature SMPs

SMPs with high glass transition temperatures therefore, high operating temperatures are desired to expand the range of possible SMP applications. Studies show that most thermally responsive shape memory epoxies have glass transition temperatures ranging between 44-98 °C [5,6,7]. Few high temperature SMPs with glass transition temperature above 100 °C are recorded in the literature. Yuyan L., Chunmiao H., Huifeng T. and Xingwen D. studied the effect of varying the content of aromatic amine curing agent in epoxy resins for application on space deployable structures [7]. Epoxy resin E-51 (WSR 618) was mixed with varying content of the curing agent DDM (4,4'-diaminodiphenyl methane). Based on DSC results, their study resulted in SMPs with glass transition temperatures of 113.5 °C and 145.3 °C when the content of the

curing agent was 90% (EP-90) and 100% (EP-100) respectively. Moreover, the study recorded the storage modulus of EP-100 at around 180 °C to be 81.7 MPa and full shape recovery of EP-90 at 180 degrees bend. After applying a Dynamic Mechanical Analysis (DMA) test, the study concluded that the highly crosslinked structure of EP-100 has greatly reduced its molecular mobility and hence, is not suitable to be used as shape memory polymer. The study then concentrated on the lower temperature SMPs resulted in reducing the curing agent content in the epoxy resin.

Moreover, researchers from NASA Glenn Research Center developed a thermally responsive thermoset Epoxy SMP with a high transformation temperature [5]. From DSC results, a glass transition temperature of 147.6 °C was obtained. In addition, DMA was used to study the crosslinking density and shape memory performance of the SMP. The focus of their research was to compare the neat epoxy SMP to a nanocomposite made by adding graphene particles. The storage modulus of the developed SMP was recorded as 1.67 GPa at 30 °C. In addition, the molecular weight and the crosslinking density were recorded. Moreover, the concentration of the DMA results was displaying the differences on deformation strains at different temperature ranges. The recovery stresses were not investigated and the recovery properties of the SMP at different loading conditions were not reported.

## Chapter 3. Materials and Methods

In this section, sample preparation and experimental procedures are discussed. A non-commercial high temperature epoxy thermoset SMP discussed in [5] was fabricated. The SMP samples were evaluated for their mechanical, shape memory and recovery properties. This section describes the method of preparing the SMP, and the various experimental techniques utilized to evaluate the material's mechanical and shape memory properties (e.g., glass transition temperature, temperature dependent modulus, and shape recovery).

### 3.1. Samples Preparation

As mentioned earlier, this work is focused on SMPs for aerospace application where high glass transition temperature is desired. The considered polymer is a high temperature epoxy based SMP originally developed by NASA [5] for potential application in morphing aircraft structures. Despite presenting comprehensive thermal assessment for the developed material, limited thermo-mechanical analysis and shape recovery characteristics were discussed. This work partially aims to address this issue by providing full experimental assessment of the thermo-mechanical and shape recovery properties of this non-commercially available SMP, henceforward referred to as EPON SMP, under various loading condition.

The EPON SMP is made by mixing 3 different chemicals which are not initially made for shape memory effect. The 3 components, purchased from Hexion Specialty Chemicals, are EPON 862, EPON 828, and the curing agent EPIKURE W. Both epoxies (EPON 862 and EPON 828) are typically used independently for fabricating composite parts, construction and aerospace adhesives, marine coatings, and molding compounds [29]. The method of fabricating the EPON SMP, shown in Figure 20, is as follows:

- 40% wt EPON 862 and 40% wt EPON 828 are poured in one beaker.
- 20% EPIKURE W is added to the mixture while stirring carefully until the solution is homogeneous. (both color and texture).
- The mixture is then degassed for 4 hours under vacuum at room temperature. This step was extremely important to remove air bubbles from the mixture and prevent porosity formation in the SMP during curing.

- Release Agent is sprayed to the mold.
- The mixture is poured to the mold and cured for 9 hours in an oven at 120°C.
- The SMP is demolded and post-cured at 150 °C for 2.5 hours.
- The SMP is cut into the needed samples using the CNC milling machine.
- All sample surfaces are polished using sandpaper of grits 600-1000 to remove excess release agent and any shape irregularities or stress concentrators.

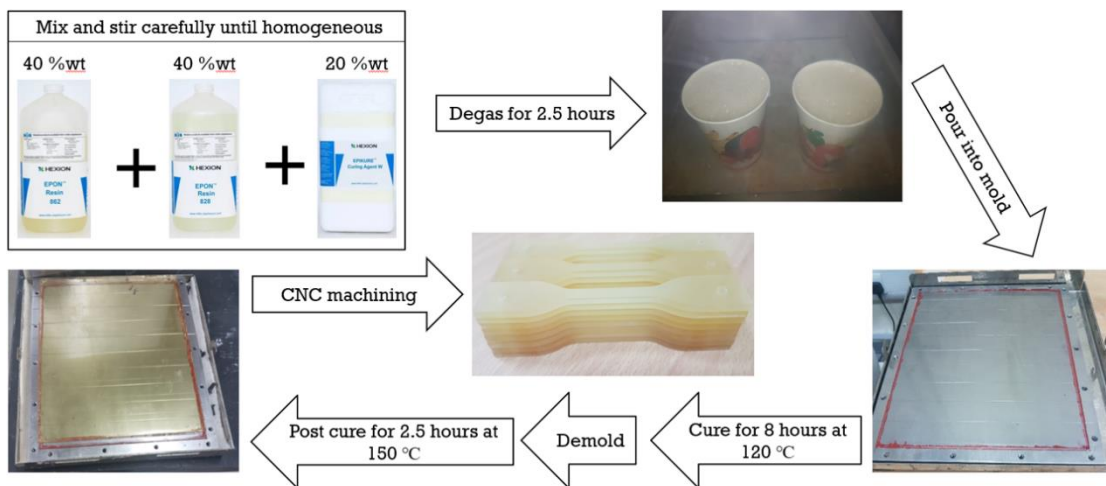


Figure 20: Sample preparation

### 3.2. Testing for Shape Memory Effect

Initial testing was conducted on the fabricated EPON SMP material to confirm successful synthesis and the presence of shape memory characteristics (*i.e.*, ensure that the polymer will recover after a being programmed into a temporary shape). The polymer was heated in a regular oven to a temperature of 180°C where it is observed to be very soft and easy to deform. Then, the sample was deformed by bending and cooled down outside the oven while maintaining the applied deformation. The sample maintained the deformed shape after cooling down and load release hence, it was successfully programmed to a temporary shape. Finally, the sample was placed back in the heated oven and recovery was observed, visually. The sample recovered to its permanent shape, initial shape, after being kept in the oven for some time (< 2 min). The programming and recovery processes are shown in Figure 21 below. The results

confirm the successful fabrication of the SMP material as shape memory effect was clearly observed in the fabricated EPON polymer.

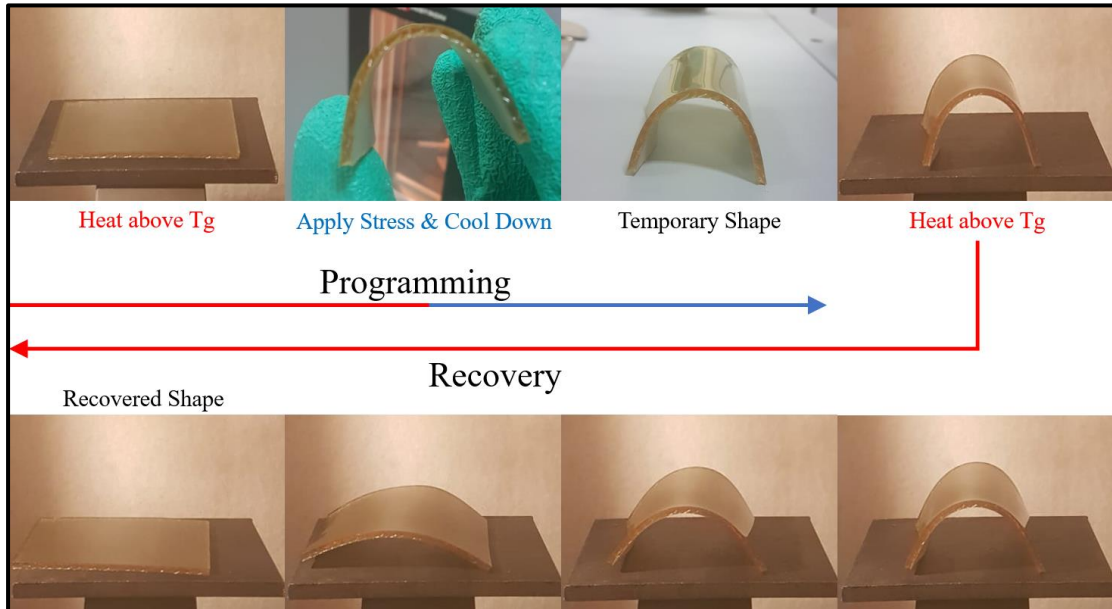


Figure 21: Programming and recovery process of SMP

### 3.3. Differential Scanning Calorimetry (DSC) Test

Knowing the glass transition temperature of the polymers is essential for this research since the shape memory effect is going to be observed beyond this temperature. A method to determine the glass transition temperature while heating or cooling the SMP is the Differential Scanning Calorimetry (DSC) test. Different batches from the EPON SMP were tested using a Perkin Elmer DSC machine. From the test, Heat Flow versus Temperature plots were obtained for the different samples and the glass transition temperatures for heating and cooling the specimen were extracted.

### 3.4. Evaluation of SMP Mechanical and Recovery Properties Using Full-Field Characterization Technique (Digital Image Correlation)

The mechanical and shape recovery properties of the EPON SMP are evaluated under Digital Image Correlation analysis. The setup included RoHS 5.0 MP Mono Grasshopper3 USB 3.0 camera and Tamron SP AF180mm F/3.5mm lens placed on a tripod and facing a universal testing machine where the samples are being tested. The

setup is shown in Figure 22 and the methods of the applied tests are explained in this section of the report.

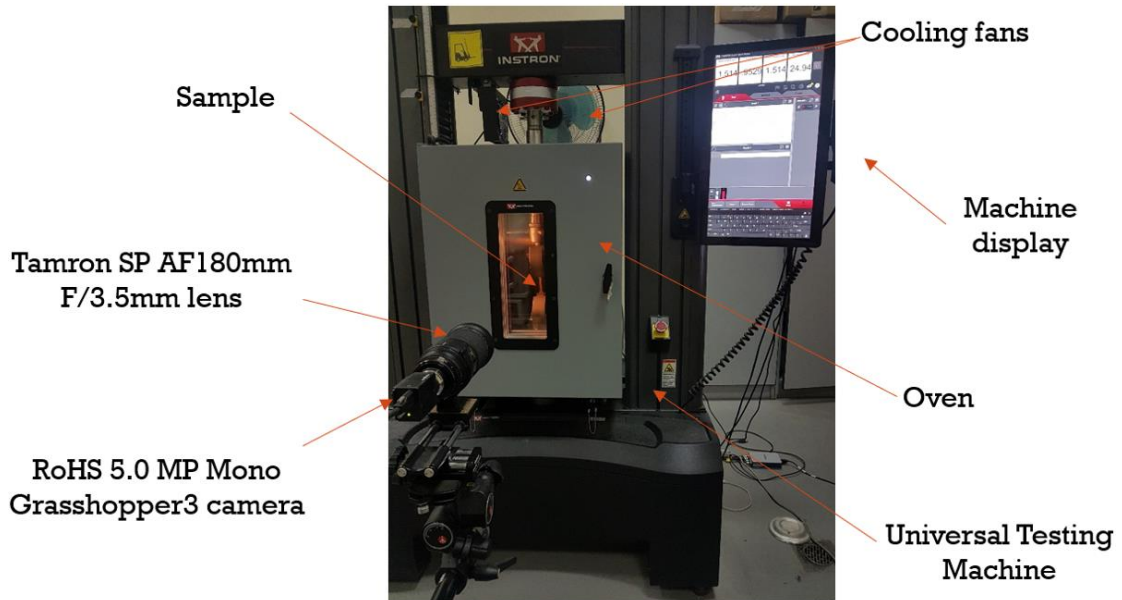


Image correlations done on Vic-2D software

Figure 22: Experimental setup

**3.4.1. Bending recovery test.** Shape memory materials recover their permanent shape from a programmed temporary shape under the exposure of external stimulus. Various parameters affect the shape recovery properties including the type of applied loading during programming the temporary shape (*i.e.*, tension, compression, bending, torsion, etc). From a practical perspective, programming under bending condition is of significant importance, in particular for morphing and deployable structures application. This type of deformation will induce complex and highly heterogeneous programmed and recovery strains. To quantify the shape memory and recovery properties of SMPs programmed in bending, a test named “bending recovery test” was conducted on samples with different geometries achieved through different bending levels (*i.e.*, bending radius and bending angle).

The different geometries are illustrated in Figure 23 and achieving the programmed shapes is explained as follows. Rectangular samples from the SMP were heated up above their glass transition temperatures, bent around a circular surface at

different radii and angles, and then cooled down while maintaining that deformation for them to fix a temporary shape. By alternating the bending angle and radius, different levels of programmed strains were introduced across the outer and inner surfaces of the investigated samples. These samples of different programmed geometries were allowed to recover freely in a pre-heated clear-glass oven. During the test, optical images of the sample's surface were captured every 1 second using RoHS 5.0 MP Mono Grasshopper3 USB 3.0 camera and Tamron SP AF180mm F/3.5mm lens. A random speckle pattern was applied on the sample's region of interest before recovery. Figure 24 shows the method of preparing the samples for the test. The optical images captured during recovery were utilized to measure the recovery response, both globally and locally using Vic-2D. In particular, the work was focused on assessing the local in-plane displacements, in-plane rotations, and strain components for the considered programming parameters (radius and angle). The different bending radii tested are 9.5mm, 6.4mm, and 3.2mm while the angles are 90 degrees and 180 degrees. The effect of recovery temperature was also evaluated by considering two different recovery temperatures of 150 °C and 200 °C.

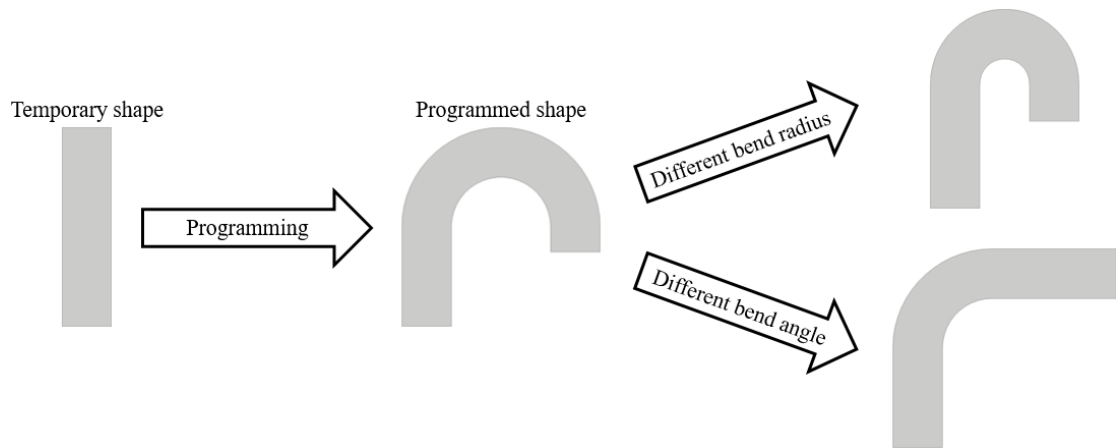


Figure 23: Different geometry samples

**3.4.2. Temperature dependent mechanical properties.** Understanding the material properties of the SMP in its glassy state (*i.e.*,  $T < T_g$ ) and in its rubbery state (*i.e.*,  $T > T_g$ ) is essential from a practical engineering and design perspective. Therefore, the EPON SMP tensile properties were evaluated at various temperatures (isothermal

experiments at RT, 50°C, 100°C, 150°C, and 180°C) above and below its glass transition temperature. The experiments were conducted on flat dog-bone shaped samples as per the description of type IV specimen in the Standard Test Method for Tensile Properties of Plastics (ASTM D638) and is shown in Figure 25. The samples were loaded in tension using an Instron Universal Testing Machine equipped with an environmental chamber. The loading rate of the test was 1 mm/min until fracture. Before running experiments at temperatures above RT, samples were soaked for 1 hour at the desired test temperature while maintaining zero stress. This step was done to ensure homogeneous sample temperature prior to deformation. During loading, optical images of the deformed sample's surface were captured every 2 seconds using RoHS 5.0 MP Mono Grasshopper3 USB 3.0 camera and Tamron SP AF180mm F/3.5mm lens. The region of interest is  $33 \times 6$  mm and the imaging resolution is 0.0119 mm/pixel. A random speckle pattern was applied on the sample's region of interest before deformation. DIC analysis was conducted using a commercially available DIC software Vic-2D. The software tracks the speckle pattern on the samples in the deformed images to measure the local in-plane displacements and calculate strain components [30]. The experimental results were used to generate stress-strain curves at the considered temperatures and evaluate the temperature dependent stiffness, yield strength (where applicable), and Poisson's ratio.

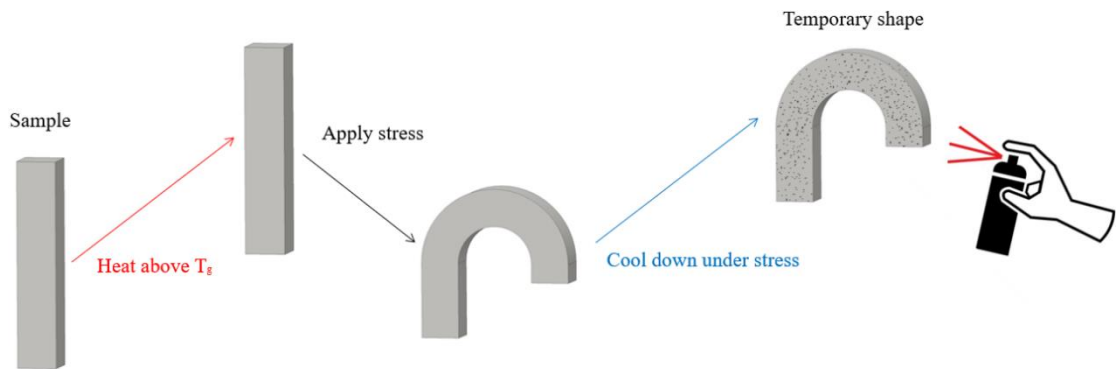


Figure 24: Bending recovery test samples preparation

**3.4.3. Stress relaxation.** Observing and understanding the stress relaxation effect on the EPON SMP is essential in evaluating the shape recovery tests. As shown in Figure 26, tensile samples were loaded in tension to 50% of their yield strain then

fixed in place for 60 minutes. After that, the grips return to their initial position and dwell for 60 more minutes. These experiments were isothermal and were conducted at RT, 50°C, and 100°C. The reaction force of the sample on the universal testing machine grips were being recorded throughout the whole experiment. The viscoelasticity of polymers causes the stress relaxation phenomenon to occur and is quantified for the EPON SMP through this experiment.

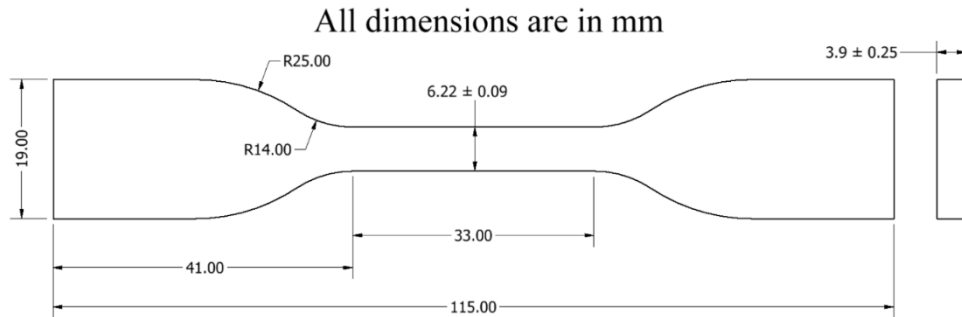


Figure 25: Tensile test sample

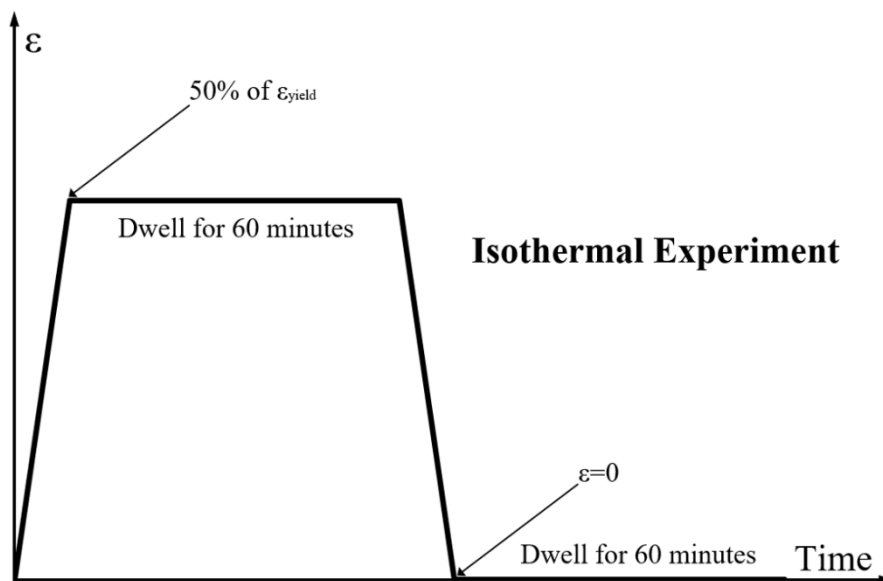


Figure 26: Stress relaxation method

**3.4.4. Stress-free tensile recovery.** SMPs unique property is that they can recover to their permanent shape from a temporary shape after being exposed to certain stimulus, temperature in this case. Evaluating this recovery under different types of

deformations is essential to further choose suitable applications. The SMP was tested for bending deformations explained previously in section 3.4.1. As for this experiment, tensile samples of the SMP were programmed under uniaxial tensile deformations using the Instron Universal Testing Machine and then allowed to recover freely at zero stress (stress-free recovery).

The samples were heated up to 180°C at a rate of 2°C/min while ensuring stress-free thermal expansion. Then, the samples were deformed at a rate of 1mm/min until reaching a stress value of 1.17 MPa. This value of stress was obtained from the extracted stress-strain graph of the SMP at 180°C in order to reach a strain of 5% for the deformed sample. The sample was then fixed in place and cooled down slowly until RT. At this stage, stresses were developing in the sample due to reduction in thermal strains under fully constrained conditions (fixed deformation). At RT, the sample was relieved from all the induced stresses and then placed in a 180°C pre-heated clear glass oven to initiate recovery and quantify the recovery strains. The sample was still placed between tensile grips in the UTM but programmed for zero stress to allow stress-free recovery.

Throughout the whole test, images were taken using RoHS 5.0 MP Mono Grasshopper3 USB 3.0 camera and Tamron SP AF180mm F/3.5mm lens to further analyze using DIC. Programming images were taken every 30s while recovery images were taken at 10s intervals. The region of interest is 33 × 6 mm and the imaging resolution is 0.0119 mm/pixel.

**3.4.5. Recovery stress.** The possibility of SMPs replacing current actuators in the aerospace industry is being studied in recent research. Having sufficient amount of force produced from the recovery process of the SMP is key to such an achievement. This section describes the procedure followed to evaluate the recovery stresses of the EPON SMP. In concept, tensile samples were programmed by introducing a certain amount of deformation then heated above  $T_g$  while constrained (fixed position) to measure the recovery stresses. Compressive stresses will initially develop due to thermal expansion however, tensile stresses will later develop at the onset of recovery.

To begin with, programmed shape was achieved by placing tensile samples in the UTM fitted with an environmental chamber and heated to 180°C at a rate of

2°C/min. The sample was then loaded to 1.17 MPa, to induce 5% strain, at a rate of 1mm/min. The sample was then fixed in place and cooled down slowly to RT. After that, the sample was relieved from the stresses induced from thermal contraction which completes the programming sequence. The recovery experiment was initiated by heating to 180°C at a rate of 2°C /min while fixed in position. The reaction forces throughout the experiment were recorded using the load cell of the UTM in order to find the recovery stresses. Throughout the experiment, images were captured every 30s using RoHS 5.0 MP Mono Grasshopper3 USB 3.0 camera and Tamron SP AF180mm F/3.5mm lens. The images were then analyzed using DIC to obtain the average strains of the sample during programming and recovery. Finally, stresses and strains during programming and recovery were plotted against temperature. Figure 27 is a graphical representation of the discussed method.

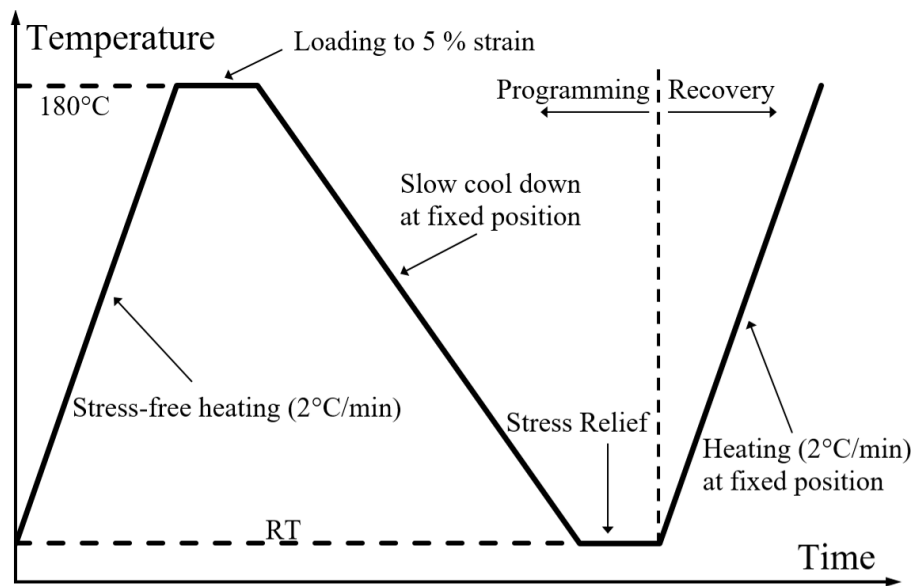


Figure 27: Recovery stress initial method

After careful analysis of the results, comparison with the literature; to be discussed in 4.6. of the report; and validating the results using the procedure discussed in section 3.4.6., it was concluded that the effect of thermal stresses and strains are clouding the recovery stress magnitudes. A modification for the previously explained recovery stress analysis method was conducted. At the final heating phase of the

experiment, the samples were heated to 110°C, relieved from all the thermal stresses induced, and then heated to 180°C at fixed position to record the recovery stresses. Figure 28 shows the modified method. This change has limited the magnitude of the developing compressive stresses due to thermal expansion and enabled less ambiguous and more reliable assessment of the recovery stress. It is important to note that the challenge arises from the high temperature properties of the considered SMP. The extremely high  $T_g$  results in significant accumulation of thermal strains before the initiation of recovery which, therefore, hinders the ability to capture the tensile recovery stress. It should be noted that the majority of SMP materials have much lower  $T_g$  (44-98 °C) [5,6,7]. and will therefore accumulate insignificant levels of thermal strains (and compressive stresses) during heating and prior to recovery.

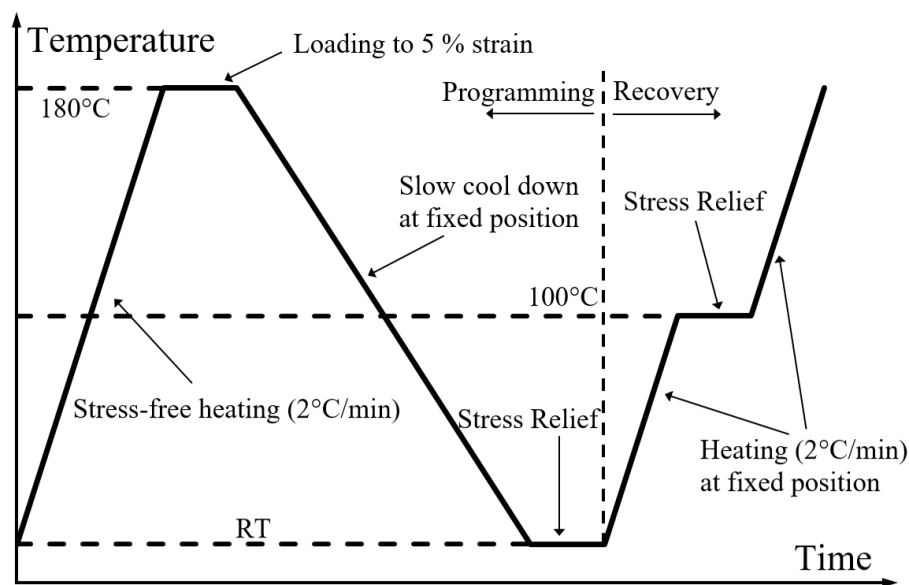


Figure 28: Recovery stress method - modified

**3.4.6. Recovery at constant stress.** The EPON SMP has a high glass transition temperature, 125°C hence, the effects of thermal stresses and strains are highly significant in the recovery process. The thermal expansion of the SMP between the grips of the universal testing machine causes a compressive reaction force. On the other hand, the recovery process causes a tensile reaction on the grips. The overlap between these reaction forces caused the validity of the recovery stress results

questionable. After further investigation, the initial results obtained from the method explained in 3.4.5. were significantly higher than the expected range of 0.05 – 4.16 MPa reported in the literature [31, 32]. In order to shed further quantitative insight into the validity of the obtained recovery stress magnitude, different recovery stress experiments were conducted. In this type of experiments, programmed samples were loaded at constant value of stress followed by heating up above  $T_g$ . The concept is that the SMP should recover if the applied stress level was less than its recovery stress. By gradually increasing the stress (each stress level requires a different sample), the applied stress will eventually exceed the recovery stress resulting in limited/no strain recovery. Although an exact recovery stress magnitude cannot be determined using this method, the upper bound or recovery stress range can be established.

Tensile samples were programmed to 5% strain using the UTM fitted with an environmental chamber. The samples were later loaded at RT to 0.5 MPa at a rate of 1mm/min. Then, the samples were heated to 180°C at a rate of 2°C/min while capturing images every 30s using RoHS 5.0 MP Mono Grasshopper3 USB 3.0 camera and Tamron SP AF180mm F/3.5mm lens. Hence, the obtained results were the strains plotted against temperature throughout the experiment. The same test was repeated at a constant stress of 2 MPa. Figure 29 is a graphical representation of the test method used on a programmed sample.

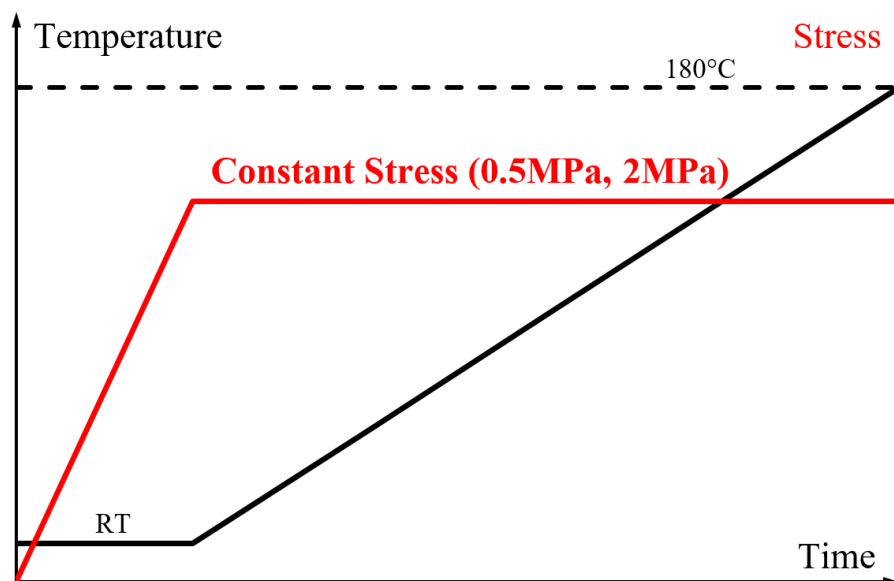


Figure 29: Recovery at constant stress method

## Chapter 4. Results and Analysis

In this chapter, the DSC test results are plotted to extract the glass transition value of the SMP. Then, the bending recovery test results are presented and discussed. Moreover, the mechanical properties and the recovery properties of the SMP at stress-free and uniaxial loading conditions are presented and discussed.

### 4.1. Differential Scanning Calorimetry (DSC) Test

DSC experiments provide heat flow measurements during heating and cooling cycles. The change in heat flow resulting from glass transition in SMPs can be captured along with the temperature at which this transition takes place (*i.e.*, glass transition temperature  $T_g$ ). Representative DSC results for the EPON SMP samples considered in this study are shown in Figure 30. The glass transition temperature was extracted during the heating and cooling cycles of the experiment. As shown in Figure 30, glass transition in the heating portion commenced once the temperature reached 110°C, and ended at around 130°C. The resulting glass transition temperature,  $T_{g,heating}$ , is therefore approximated to be around 125°C. By following a similar approach during the cooling cycle, the glass transition temperature,  $T_{g,cooling}$ , was approximated to be around 130°C. In summary, the DSC measurements collected from EPON SMP samples (total of 3 samples) point to a glass transition region expanding between ~ 110 and 140 °C with an average glass transition temperature  $T_g$  of 125°C ( $\pm 5^\circ\text{C}$ ).

### 4.2. Bending Recovery Test

The recovery of non-uniformly deformed (*i.e.* bending) SMPs was analyzed by assessing the local in-plane displacements, in-plane rotations, and strain components for SMP samples exposed to different programming levels. As mentioned previously in 3.4.1. and shown in Figures 23 and 24, a random speckle pattern was sprayed on SMP samples programmed at different levels. Furthermore, recovery images were taken during the SMP recovery process and correlated using the commercial software Vic-2D hence, DIC technique. The software tracked the random speckle pattern in the specified region of interest across the recovery images to extract the following data: horizontal displacements ( $U$ ), vertical displacements ( $V$ ), lagrangian strains along the x-axis ( $\epsilon_{xx}$ ), lagrangian strains along the y-axis ( $\epsilon_{yy}$ ), lagrangian shear strains ( $\epsilon_{xy}$ ), major principal strains ( $\epsilon_1$ ), minor principal strains ( $\epsilon_2$ ), and in-plane rotations ( $\phi$ ). Contour

plots were obtained for each of the parameters mentioned and a schematic showing the recovery process along with the extracted contour plots is shown in Figure 31.

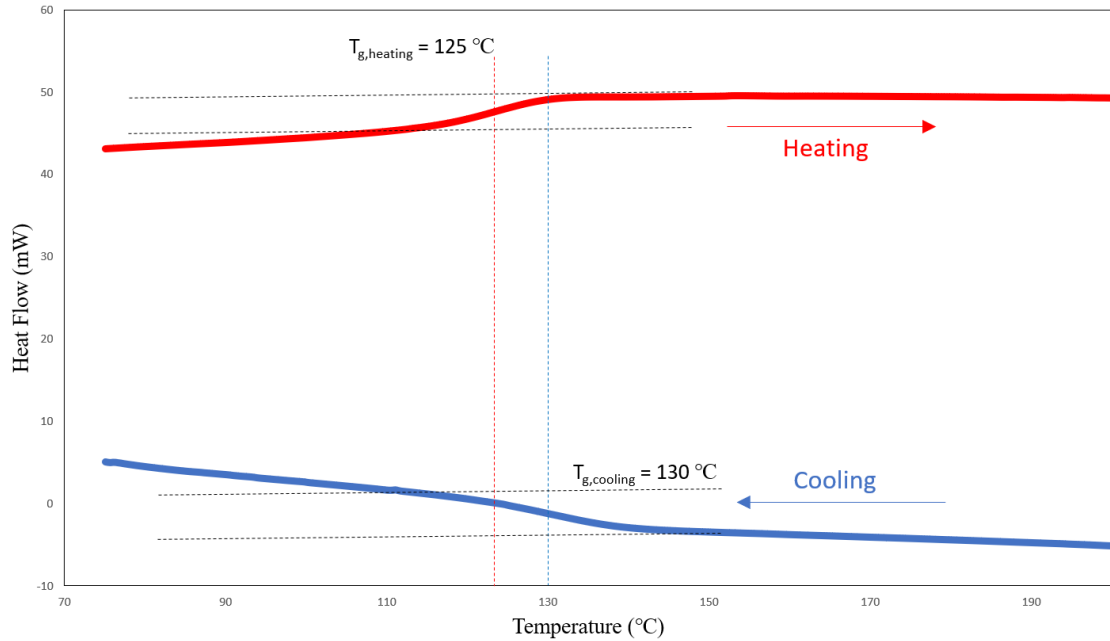


Figure 30: DSC test result - EPON SMP

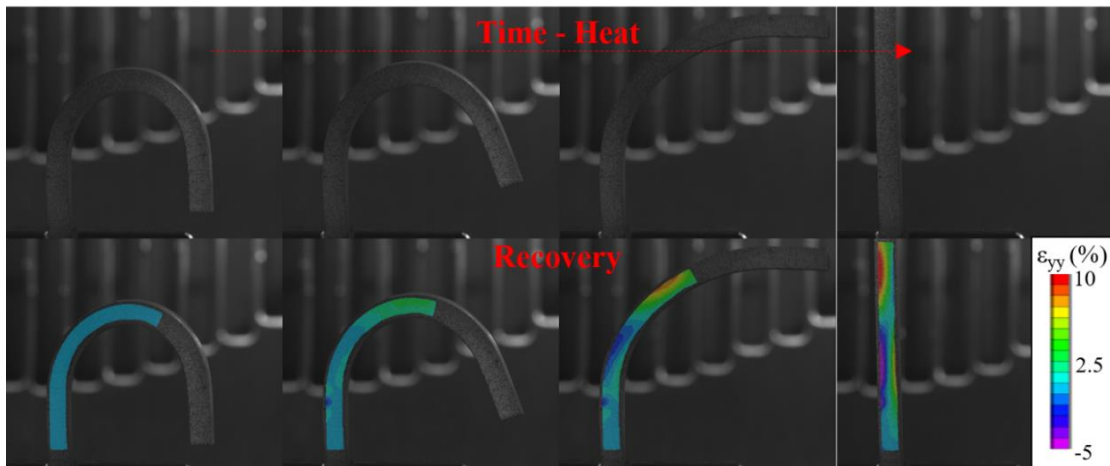


Figure 31: EPON recovery

Since the applied deformation is non-uniform (bending), the recovery of the SMP was observed to be heterogeneous. Therefore, to study the effect of different deformation levels on the recovery process, different regions highlighted in Figure 32

were chosen for the analysis. The mean values of the local in-plane displacements, in-plane rotations, and strain components in each region were measured using Vic-2D. The regions specified for all samples are as follows: near the grip where the sample was supported (A), a region before the center of the applied deformation (B), and the center of the deformation (C). It is important to note that the deformation level increases by going from region A to C. Moreover, the recovery process starts after reaching the glass transition temperature and ends by recovering to the SMP's permanent shape prior to programming.

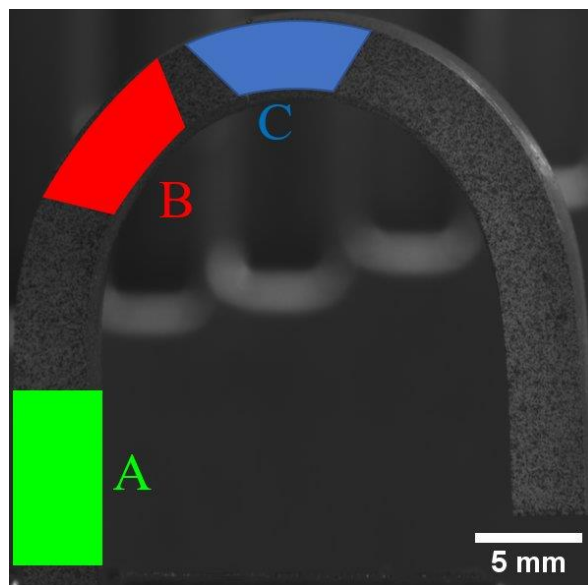


Figure 32: Analyzed regions

Figure 33 shows the recovered horizontal displacements of a sample in the aforementioned regions. It was observed from Figure 33 that the recovered horizontal displacement accelerated to a constant rate for each region and then decelerated to rest. The horizontal displacement rates of recovery were calculated from the slopes of the curves as shown in Figure 33. Based on Vic-2D coordinates, the horizontal displacement readings were recorded as negative values since the samples were recovering to the left. The horizontal displacement recovery rate of A was almost zero since the deformation level was insignificant in this region prior to recovery. However, region C which had the highest amount of deformation applied had the fastest horizontal

displacement recovery rate (0.688 mm/s). Moreover, region B experienced a horizontal displacement recovery rate of 0.12 mm/s.

To be able to validate the results obtained from the DIC analysis, a drawing software named Fiji was used. A point on the sample's surface was traced from the beginning of the test until the end using the optical images captured during recovery. The reference image of the test (programmed shape) and the last photo taken after completion of the test (recovered shape) were placed in parallel as shown in the Figure 34. The software Fiji was used to measure the horizontal distance that the point travelled due to recovery and to compare it with the value obtained from Vic-2D. The difference between the horizontal displacement value obtained from Vic-2D and the one obtained from Fiji was 2.33% which showed good correspondence between the two methods.

$$\%Difference = \frac{17.0856 - 16.696}{16.696} \times 100\% = 2.33\% \quad (4)$$

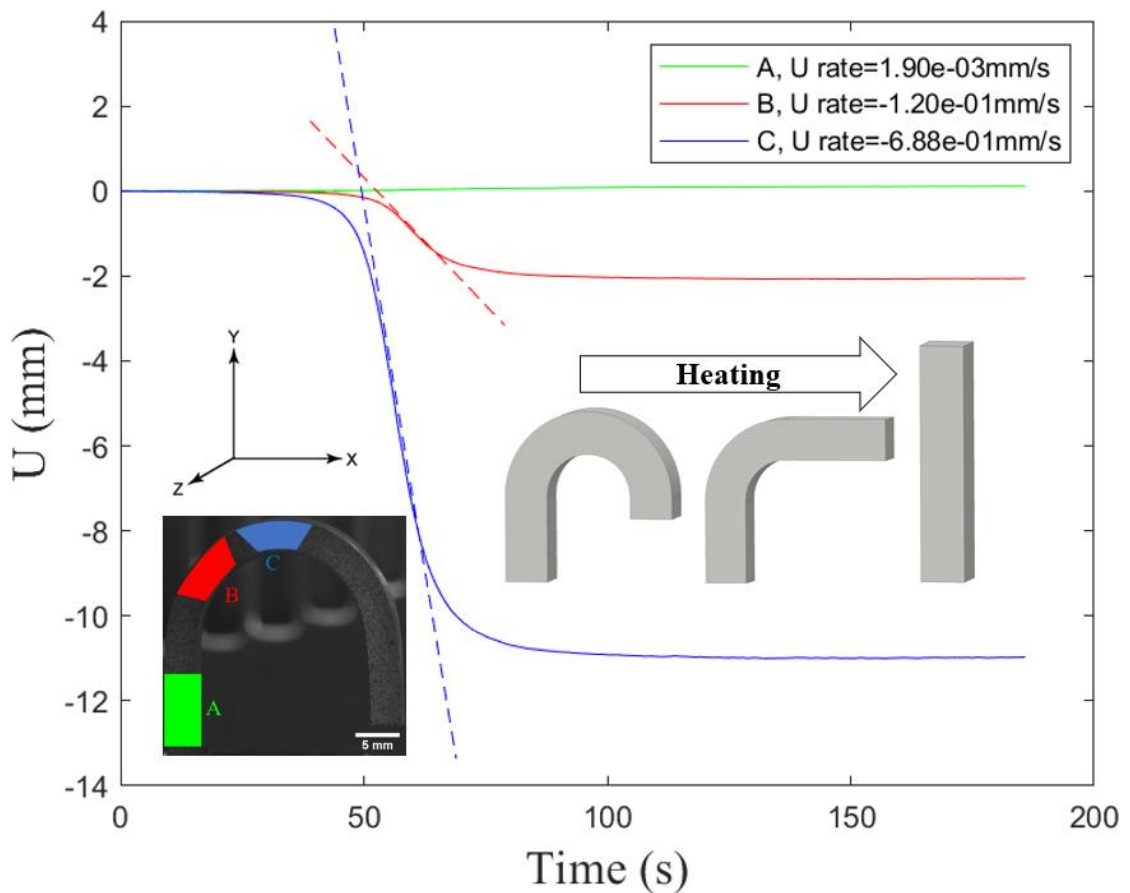


Figure 33: EPON sample horizontal displacement vs. time

Figure 35 shows the recovered vertical displacements of the sample in the same regions illustrated in Figure 32. Similar to the trend observed for the horizontal displacements recovery, it is shown in Figure 35 that the recovered vertical displacement accelerated to a constant rate for each region and then decelerated to rest. The vertical displacement recovery rates were calculated from the slopes of the curves as shown in Figure 35. It was observed that the vertical displacements recovery curves followed a similar trend to the horizontal displacements' recovery. Region A did not experience recovery while region C recovered with a rate of 0.449 mm/s. In addition, the vertical displacement recovery rate of region B was recorded as 0.0336 mm/s.

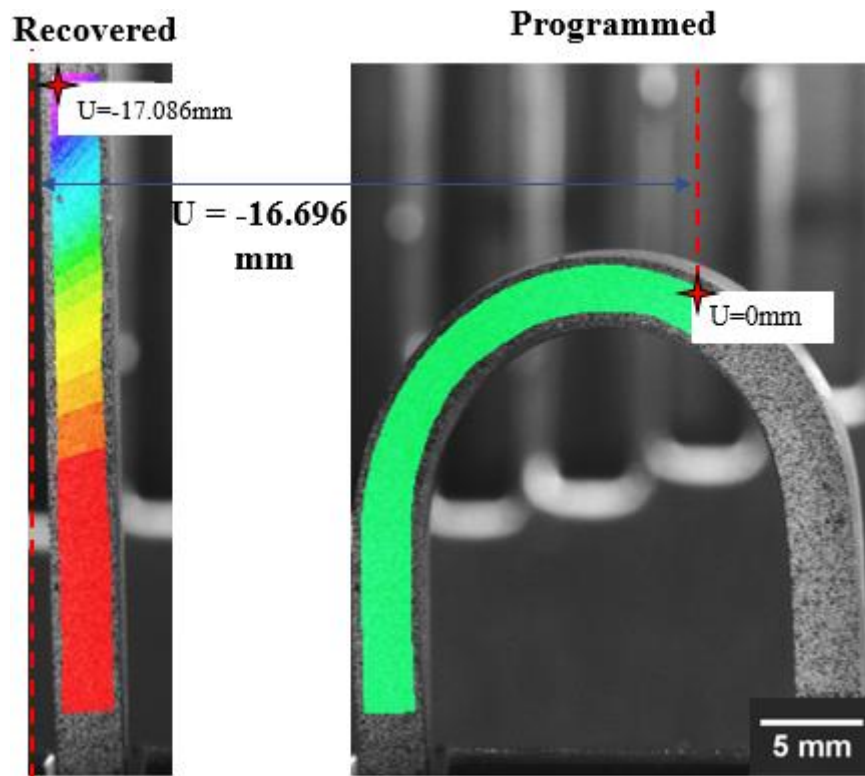


Figure 34: Horizontal displacement ( $U$ ) validation

The recovered vertical displacements measured by Vic-2D were also validated using the software Fiji. The same point on the sample's surface was traced from the beginning of the test until the end (*i.e.*, until full recovery). The images used and the traced point are shown in Figure 36. Moreover, the difference between the vertical displacement value obtained from Vic-2D and the one obtained from Fiji was 3.07% which validated the results extracted from Vic-2D and are shown in Figure 35.

$$\%Difference = \frac{10.5671 - 10.252}{10.252} \times 100\% = 3.07\% \quad (5)$$

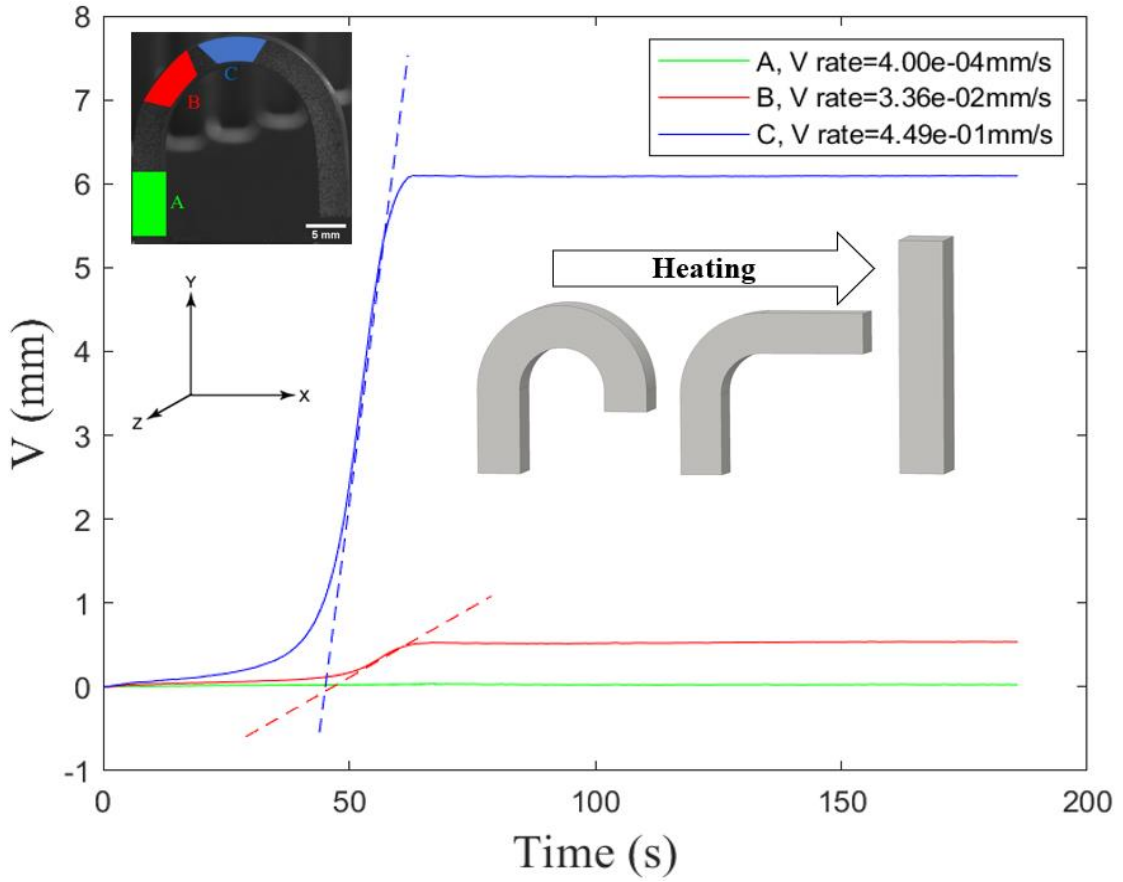


Figure 35: EPON sample vertical displacement vs. time

To evaluate the recovered strain at different regions across the samples, the equivalent von-mises strain was calculated and plotted against time. The von-mises strain was calculated using the following equation [33]:

$$\varepsilon_v = \sqrt{\varepsilon_1^2 - \varepsilon_1\varepsilon_2 + \varepsilon_2^2} \quad (6)$$

where  $\varepsilon_1$  is the major principal strain and  $\varepsilon_2$  is the minor principal strain. Moreover, the major and minor principal strains are related to the lagrangian strains along the x-axis, lagrangian strains along the y-axis, and lagrangian shear strains as follows [34]:

$$\varepsilon_1, \varepsilon_2 = \frac{\varepsilon_{xx} + \varepsilon_{yy}}{2} \pm \sqrt{\left(\frac{\varepsilon_{xx} - \varepsilon_{yy}}{2}\right)^2 + \left(\frac{\varepsilon_{xy}}{2}\right)^2} \quad (7)$$

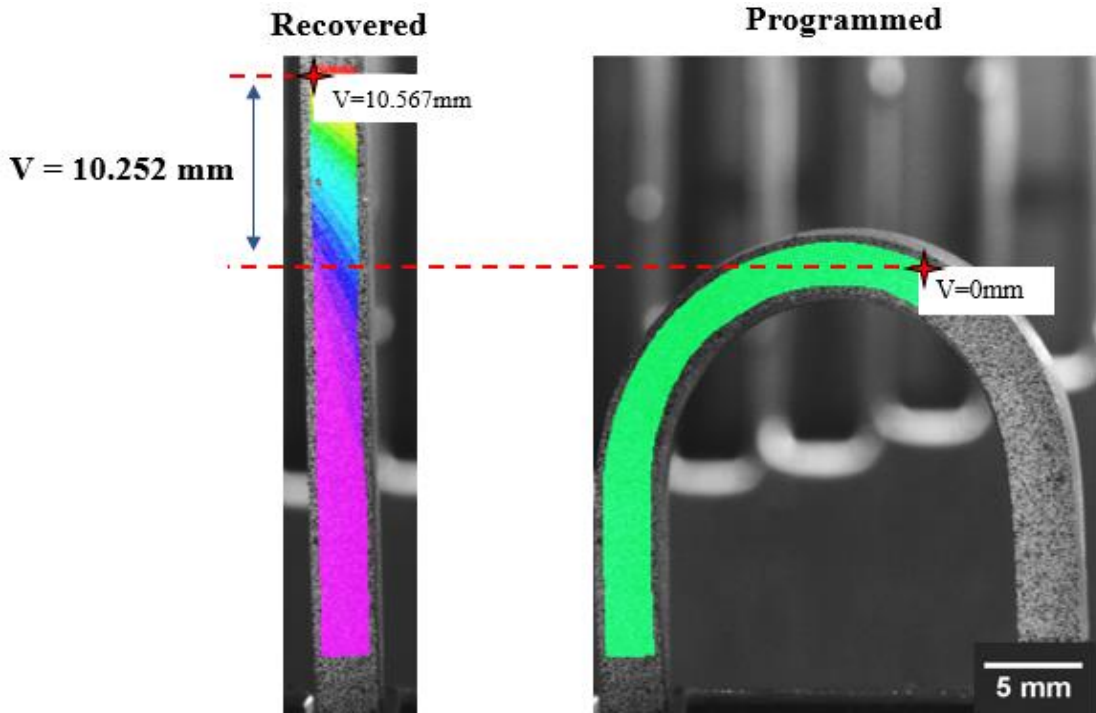


Figure 36: Vertical displacement ( $V$ ) validation

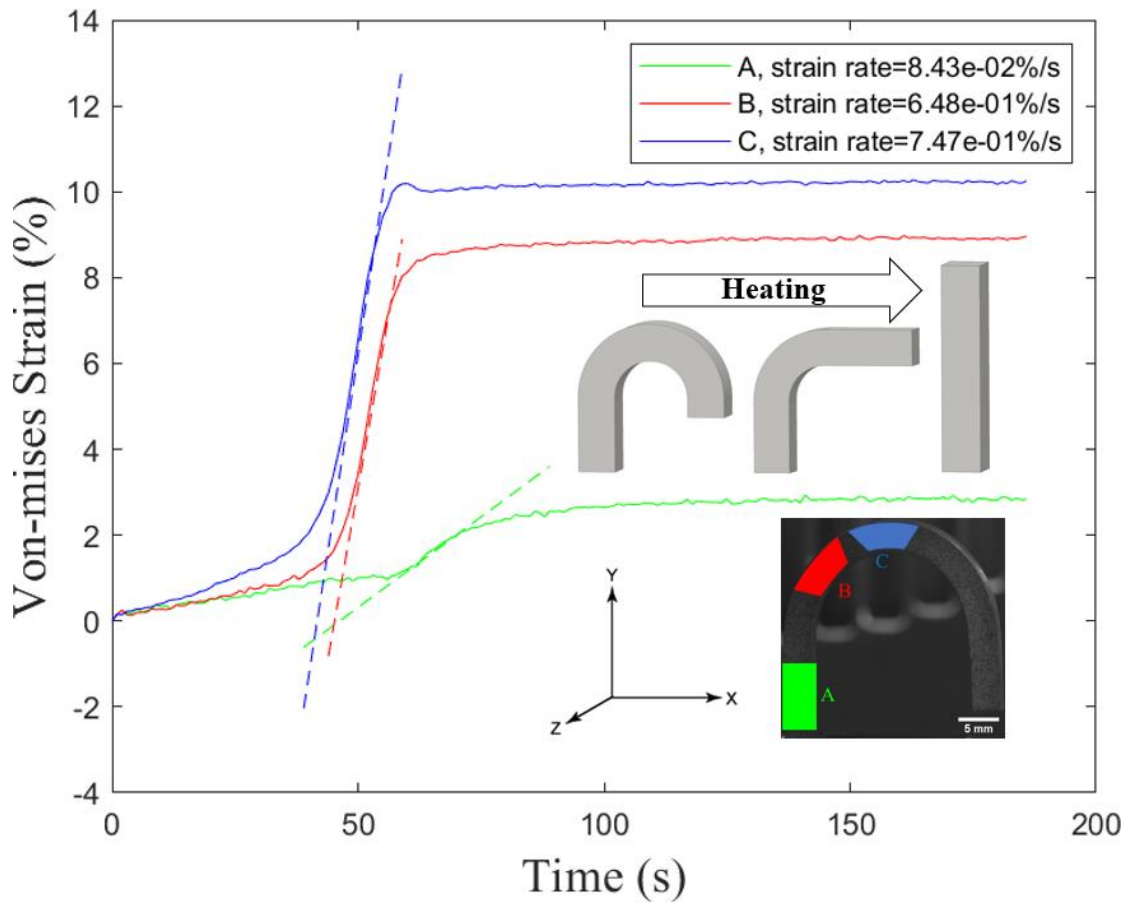


Figure 37: EPON sample von-mises strain vs. time

Figure 37 shows that the recovered von-mises strain values accelerated to a constant rate for each region and then decelerated to rest. The von-mises strain rate of recovery was also calculated from the slopes of the curves shown in Figure 37. The recovery rate of region A was very small (0.084 %/s) when compared to the other regions and the maximum recovered strain was found to be less than 3%. On the other hand, region C had the highest magnitude of recovered strain (around 10 %) since it experienced the highest level of deformation prior to recovery. Moreover, region C experienced the fastest von-mises strain rate of recovery of around 0.747 %/s. It is important to note that there was no need to validate the recovered von-mises strain values since they were extracted from the validated horizontal displacements (U) and the vertical displacements (V). As shown previously in equations 6 and 7, the von-mises strains were calculated using the major and minor principal strains values. Moreover, the principal strains were calculated using the lagrangian strains which were computed by Vic-2D software as follows [33]:

$$\varepsilon_{xx} = \frac{\partial u}{\partial x} + \frac{\left(\frac{\partial u}{\partial x}\right)^2 + \left(\frac{\partial v}{\partial x}\right)^2}{2} \quad (8)$$

$$\varepsilon_{yy} = \frac{\partial v}{\partial y} + \frac{\left(\frac{\partial u}{\partial y}\right)^2 + \left(\frac{\partial v}{\partial y}\right)^2}{2} \quad (9)$$

$$\varepsilon_{xy} = \frac{\frac{\partial u}{\partial y} + \frac{\partial v}{\partial x} + \frac{\partial u}{\partial x} \frac{\partial u}{\partial y} + \frac{\partial v}{\partial x} \frac{\partial v}{\partial y}}{2} \quad (10)$$

Furthermore, the in-plane rotations of the samples at the previously mentioned regions were evaluated. The deformation of the samples was heterogeneous and was applied by bending the samples on a circular arc surface of either 90° or 180°. Hence, measuring the in-plane rotation angles of the different regions across the samples indicated the percentage recovery of the SMP. Figure 38 shows the in-plane rotations of the SMP sample at regions A, B, and C. Moreover, the instants where the SMP recovered 80%, 90%, and 100% of the applied deformation across each region were labelled. It is important to note that Figure 38 was plotted for a sample bent over a 180° circular arc surface. Nevertheless, and due to the limitations in the field of view of the camera lens used, the SMP recovered images did not include any region further than region C. Moreover, region C experienced around 90° local in-plane rotation and reached a state of 100% recovery after around 80s from the start of the experiment.

The rotation angle values computed by Vic-2D were also validated using the drawing software Fiji. A line was traced from the beginning of the test until the end using Vic-2D. The reference image of the test (programmed shape) and the last photo taken after completion of the test (recovered shape) were compared as shown in Figure 39. The software Fiji was used to measure the rotation angle of the line after recovery and compare it with the angle measured by Vic-2D. The two methods displayed good correspondence with a percentage difference of 1.04%.

$$\%Difference = \frac{1.608 - 1.5913}{1.608} \times 100\% = 1.04\% \quad (11)$$

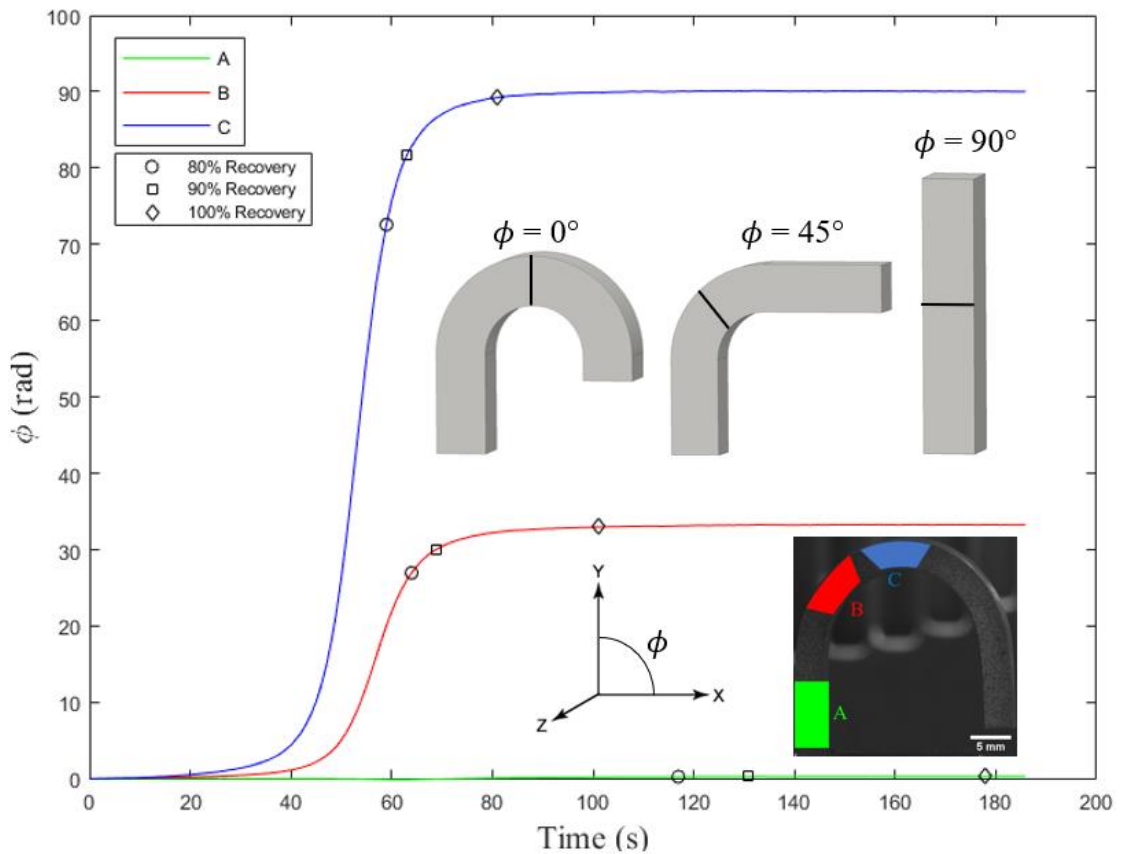


Figure 38: EPON sample in-plane rotation angle vs. time

The analysis discussed earlier was for the sample EPON-018 which was bent on a circular arc surface of radius 9.5 mm and at an angle of 180°. Moreover, the recovery temperature of EPON-018 was 200°C. Nonetheless, the same analysis was conducted on EPON SMP samples recovering at different temperatures (150°C, and

200°C) and having different programmed geometries (*i.e.* bending radius, bending angle). The recovery was evaluated for the different samples and comparison Figures 40, 41, 42 and 43 were generated. The aim of these Figures was to investigate any possible trends in the recovery behavior of the SMP samples while changing the deformation level or the recovery temperature. Region A was excluded from the comparison since it experienced no significant deformation. The samples in each Figure were ordered based on the different bending radii tested, different bend angles, and different recovery temperatures. The bending radii are ordered starting with the highest value (R=9.5 mm) at the left, and the lowest value (R=3.2 mm) at the far right. The red and blue highlights indicate recovery temperatures of 200°C and 150°C respectively. Moreover, the shape of the samples shown on the Figures indicate the different bend angles (180° and 90°).

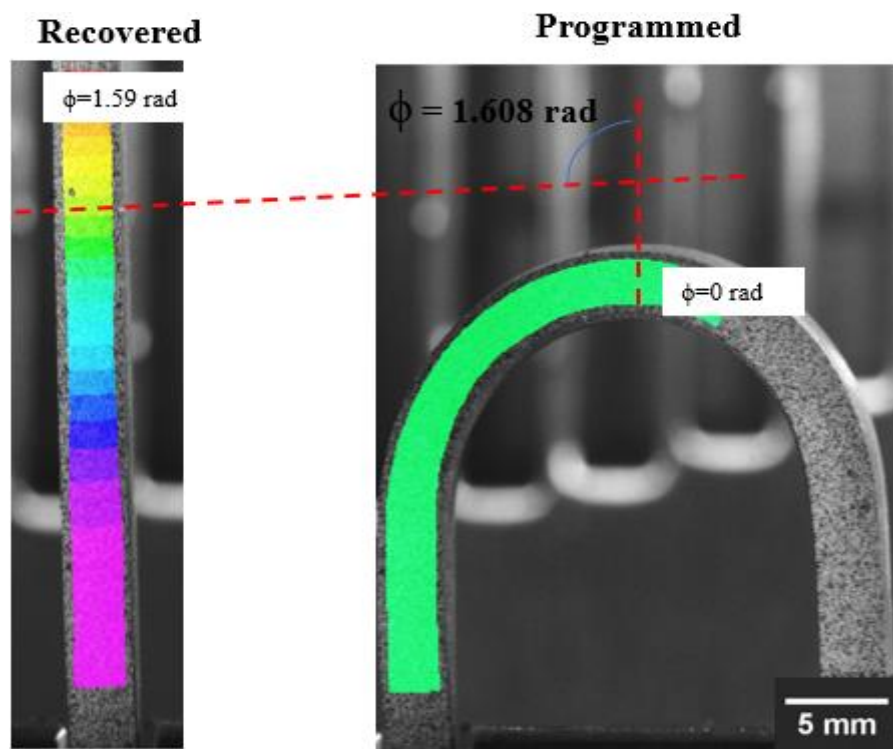


Figure 39: Rotation angle validation

From Figures 40, 41, 42 and 43, it was observed that the SMP recovery is highly dependent on the bending angle, bending radius, and recovery temperature. Changing those parameters reflected on the horizontal displacement, vertical displacement, and

von-mises strain recovery rates. Based on Figure 43, it was observed that the relationship between changing the bending radius or the bending angle to the time needed for full recovery was not very consistent. The comparison needed further investigation which was conducted and explained later in this section of the report. On the other hand, it was observed that the samples tested at a higher oven temperature needed less time for 100% recovery. To be able to quantify and study the relationship between the aforementioned parameters on the recovery process, region C was chosen since it had the highest applied deformation in all samples. The horizontal displacement, vertical displacement, and von-mises strain curves for region C for samples of different geometries were plotted and compared in Figures 44, 45, 46, 47, 48, 49, 50, 51, and 52.

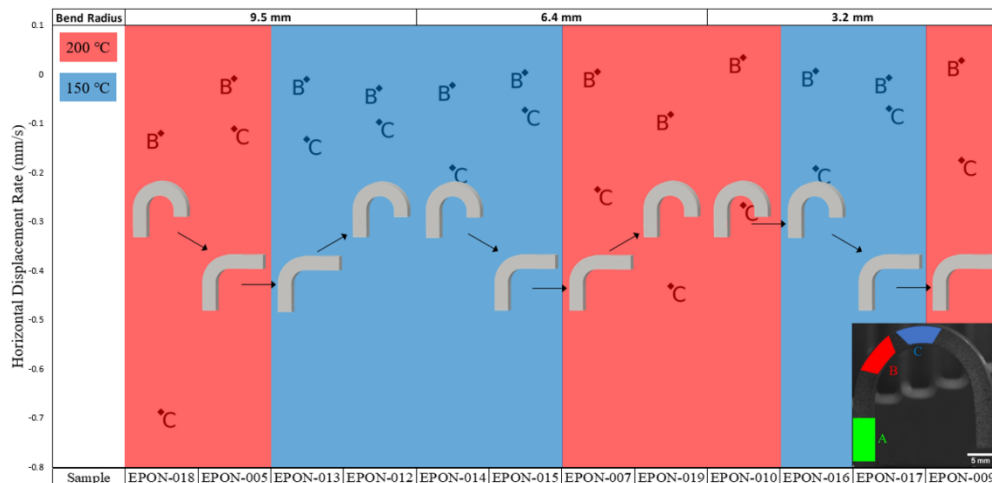


Figure 40: EPON samples comparison - Horizontal displacement rate

Based on Figures 44,45, and 46, it was observed that increasing the bending angle increased the recovery rates of the horizontal displacement, vertical displacement, and the von-mises strain. In addition, and since the deformation level was higher in the 180° bent samples than the 90° bent samples, the magnitudes of the recovered displacements and strain were higher. Moreover, it was observed that the 180° samples needed less time to complete the recovery process even though the magnitude of the deformation was higher.

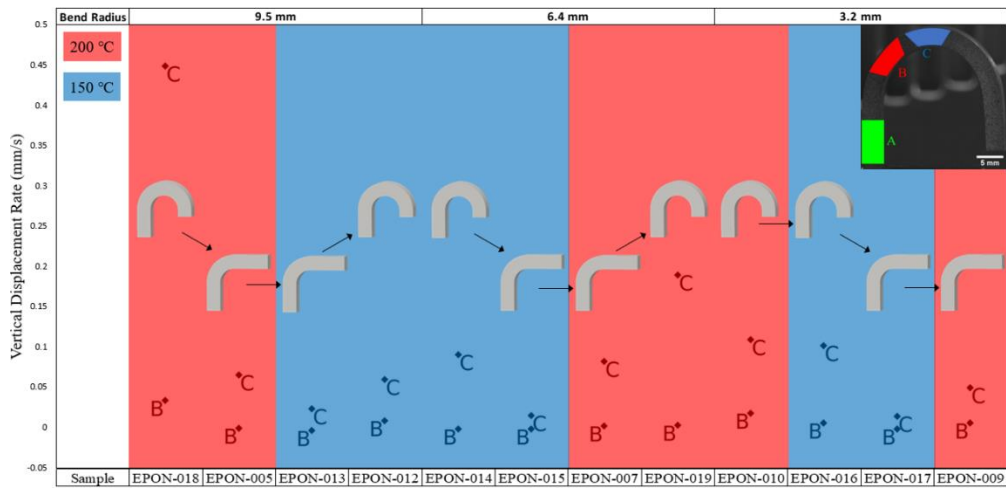


Figure 41: EPON samples comparison - vertical displacement rate

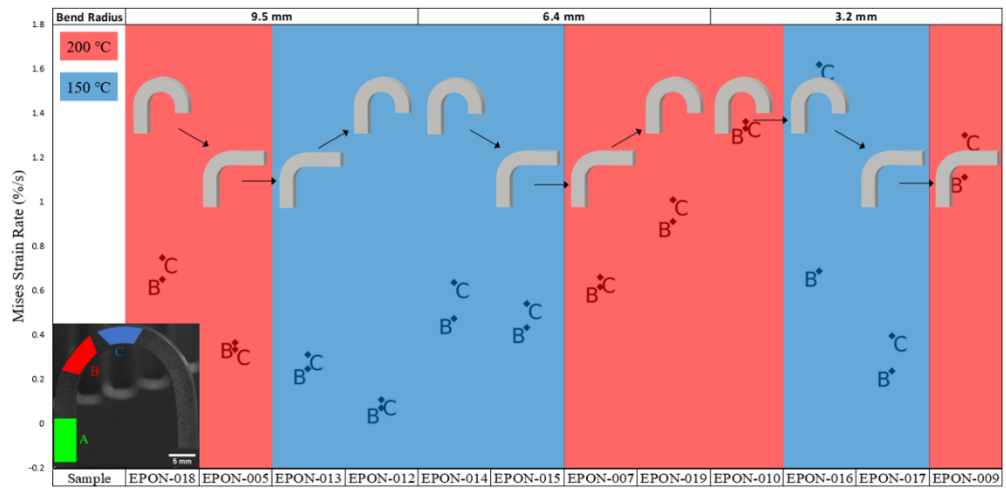


Figure 42: EPON samples comparison – von-mises strain rate

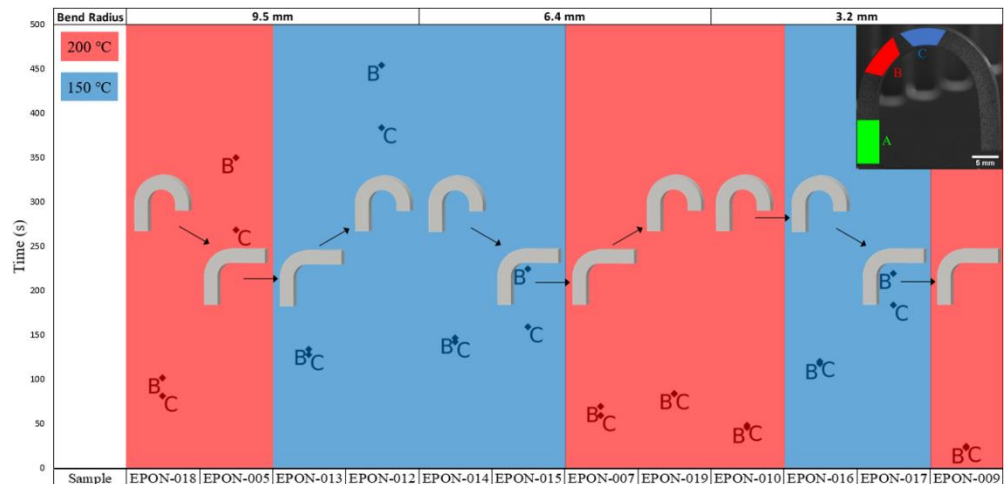


Figure 43: EPON samples comparison - time to 100% recovery

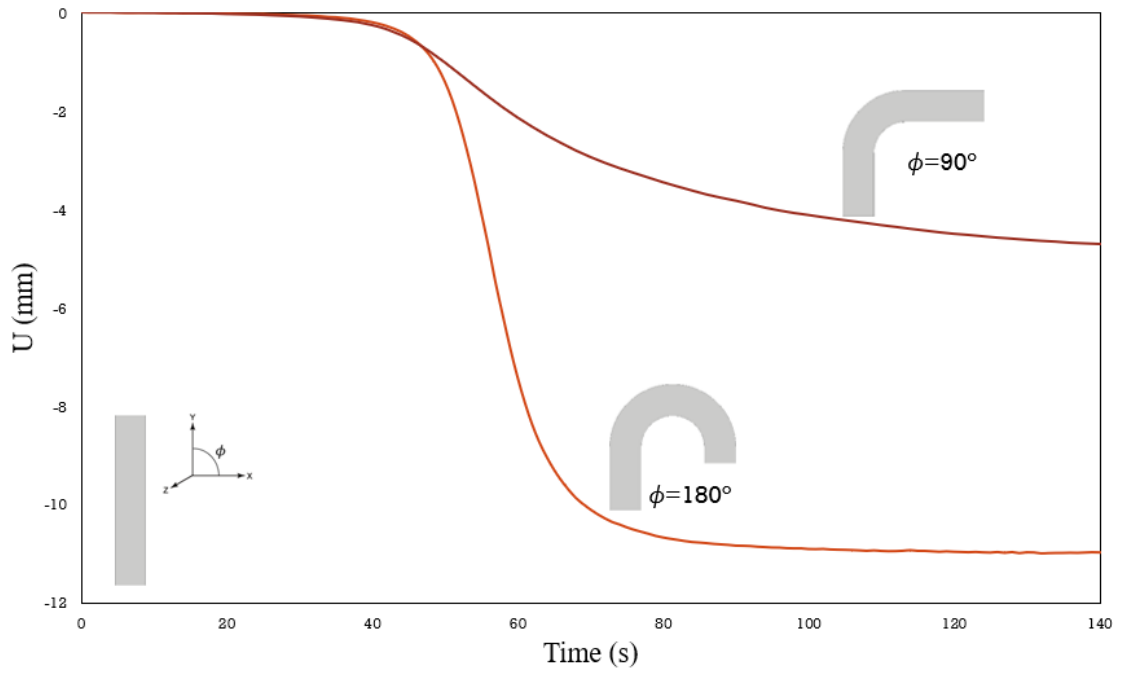


Figure 44: Different bending angles comparison - horizontal displacement

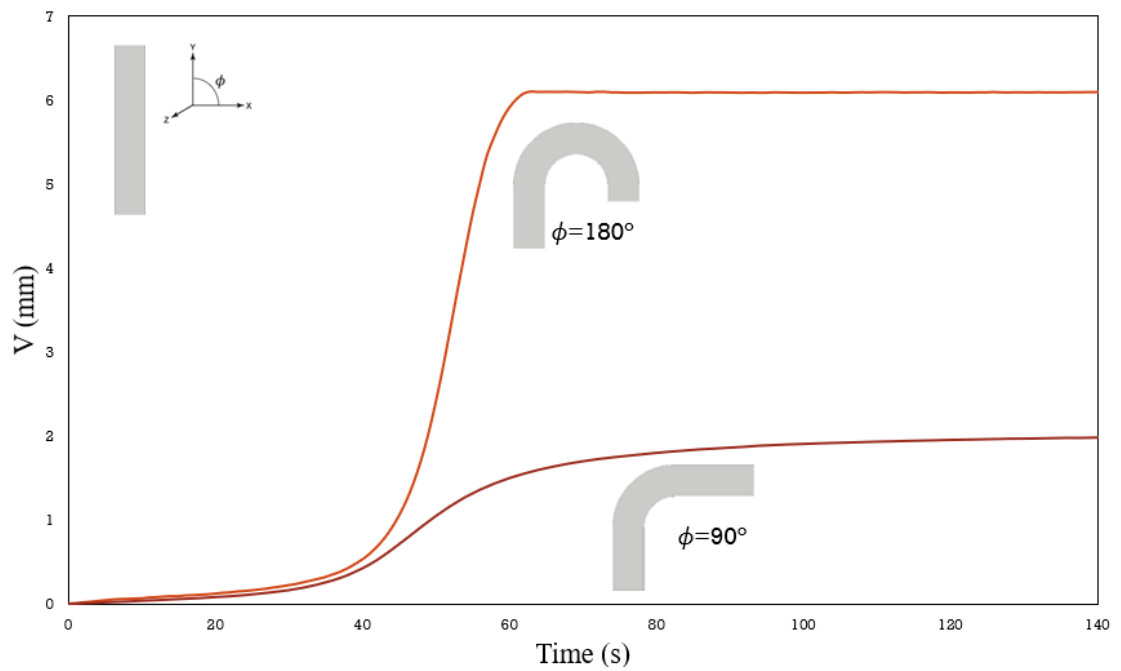


Figure 45: Different bending angles comparison - vertical displacement

Based on Figures 47, 48, and 49, it was observed that decreasing the bending radius, hence a higher deformation strain, increased the strain recovery rate.

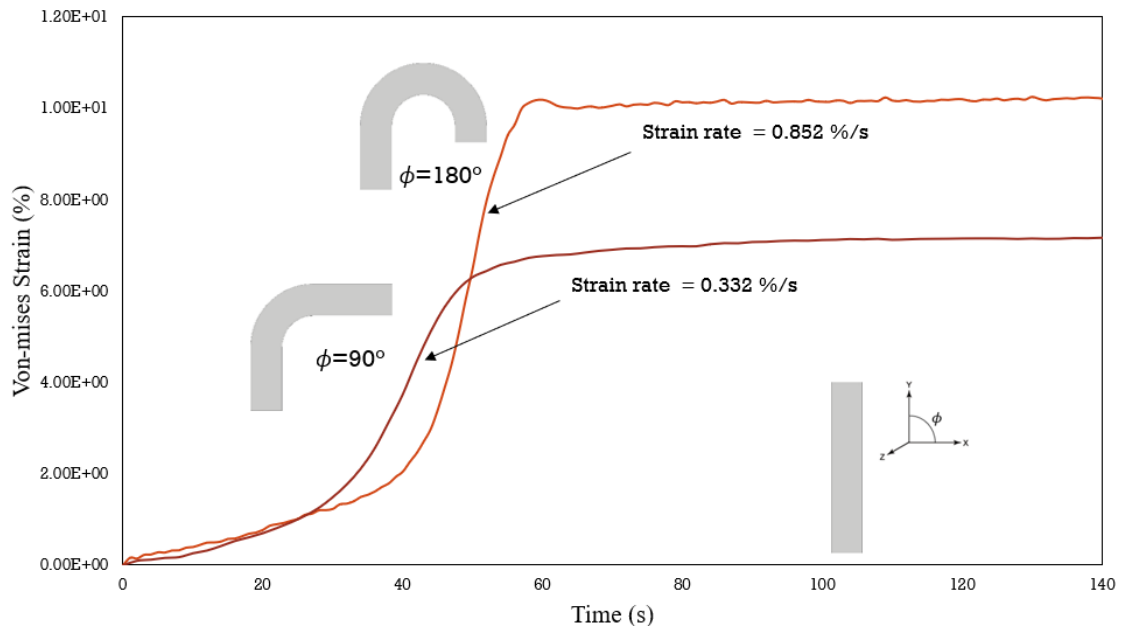


Figure 46: Different bending angles comparison - von-mises strain

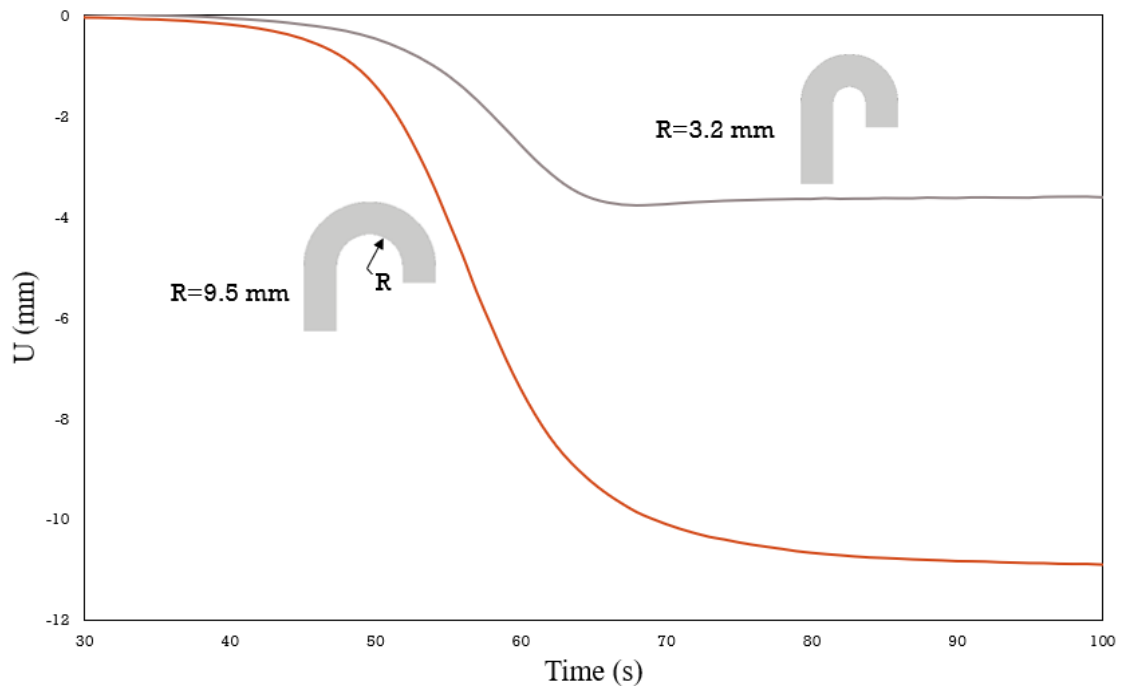


Figure 47: Different bending radii comparison - horizontal displacement

Based on Figures 50, 51, and 52, it was observed that decreasing the oven temperature delayed the start of recovery. Also, decreasing the temperature of the oven decreased the recovery rate of the samples. It was concluded from the bending recovery

experiments that the SMP recovery is dependent on programmed strain and recovery temperature. The higher the programmed strain, the higher strain recovery rate. Moreover, higher recovery temperatures speed up the recovery process significantly.

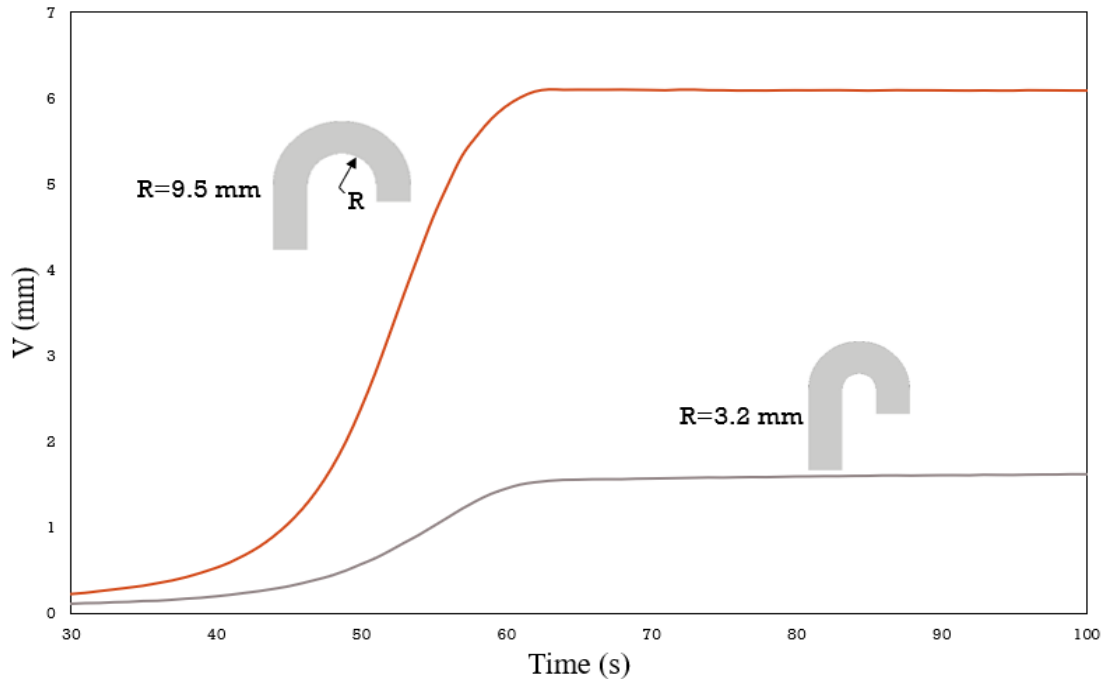


Figure 48: Different bending radii comparison - vertical displacement

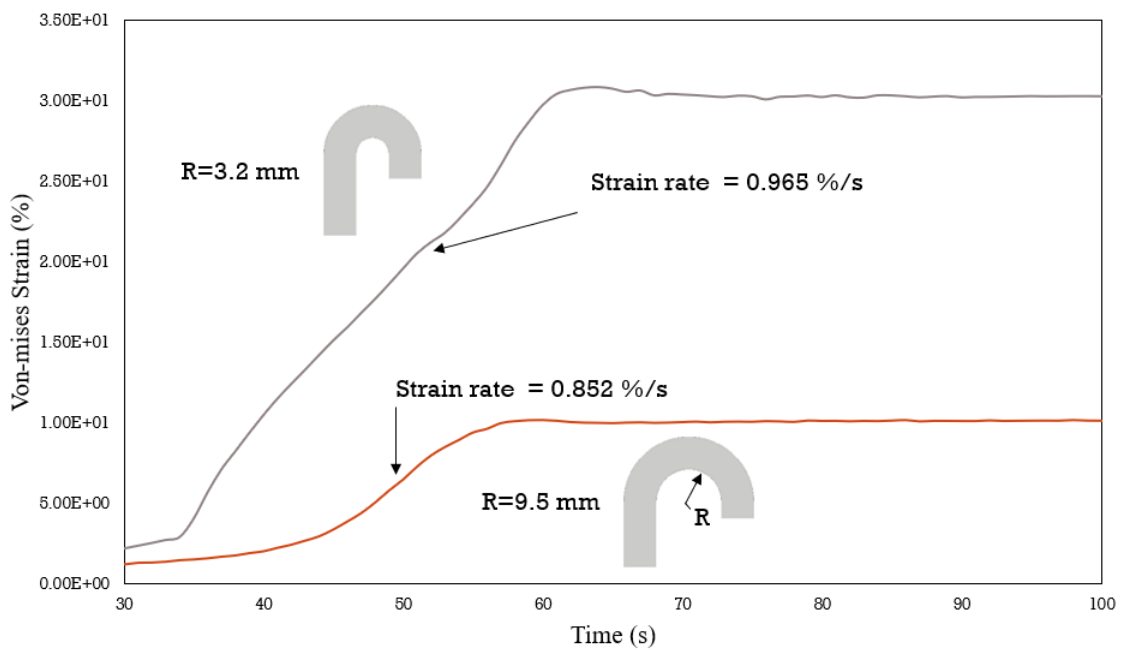


Figure 49: Different bending radii comparison - von-mises strain

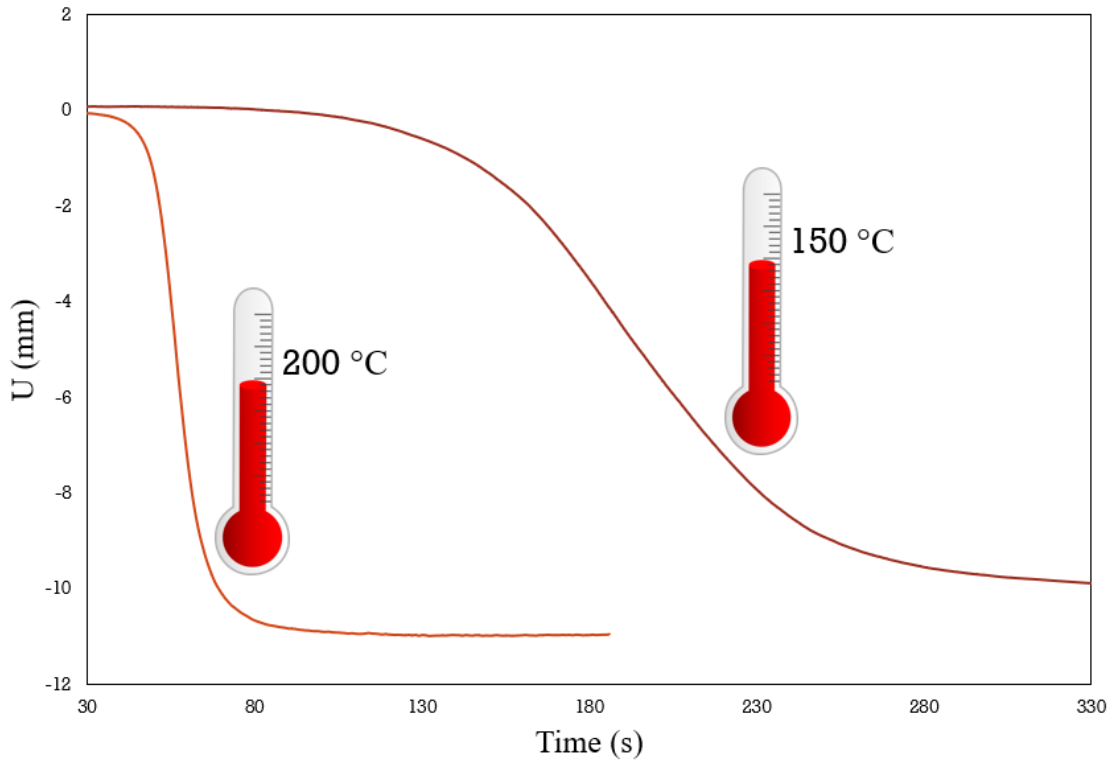


Figure 50: Different oven temperature comparison - horizontal displacement

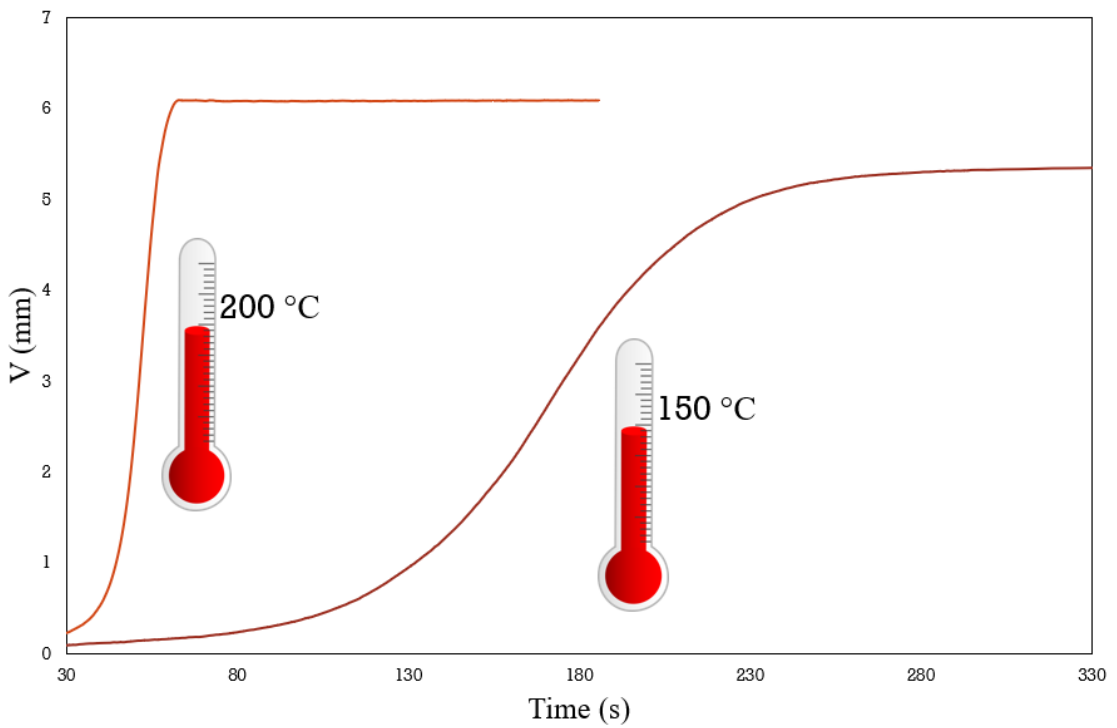


Figure 51: Different oven temperature comparison - vertical displacement

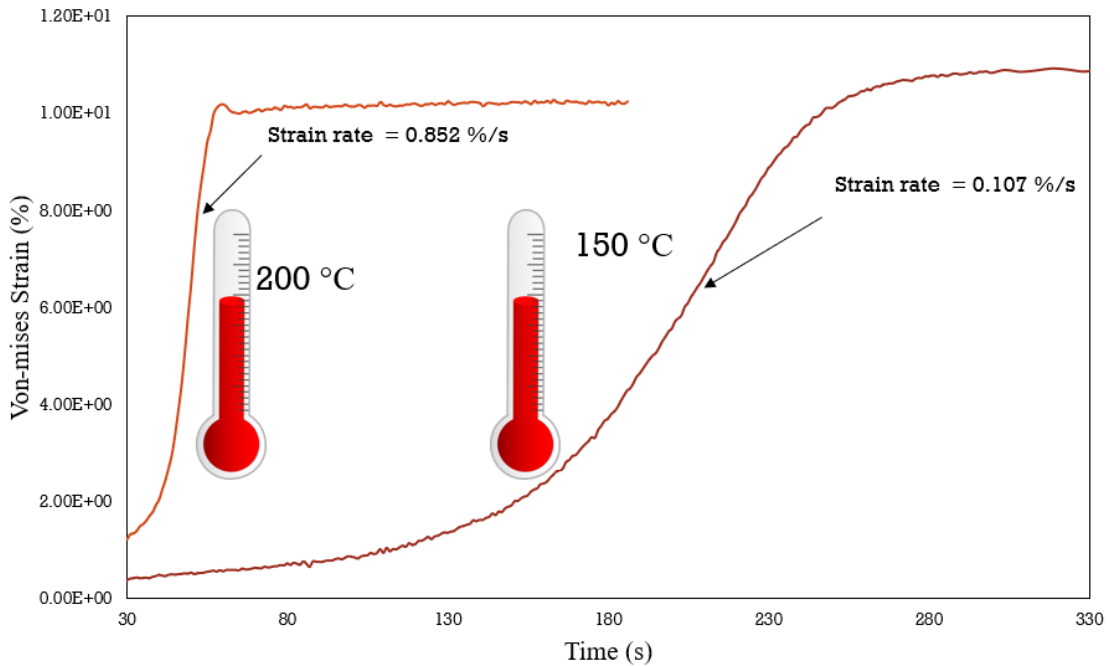


Figure 52: Different oven temperature comparison - von-mises strain

### 4.3. Temperature Dependent Mechanical Properties

The tensile experiments were conducted at different temperatures for the EPON SMP samples as discussed previously in section 3.4.2. of this report. Figure 53 shows the representative stress versus strain curves obtained at various deformation temperatures (isothermal experiments), both below and above the glass transition temperature of the EPON SMP material. The stress-strain curves obtained at deformation temperatures below  $T_g$  (*i.e.*, RT, 50, and 100 °C) show a typical plastic behavior with yielding at the maximum stress followed by softening response. The elastic modulus ( $E$ ) and yield strength both decreased, as expected, with temperature increase while the ductility improved. The data collected beyond the glass transition temperature ( $T_g = 125^\circ\text{C}$ ), showed a significant change in mechanical properties with large drop in strength, stiffness (drop by a factor of  $\sim 100$ ), and primarily a linear response up to fracture. As for the tensile test at  $180^\circ\text{C}$ , the shape of the stress-strain graph is similar to the one at  $150^\circ\text{C}$ . However, the elastic modulus slightly increased and the strain at fracture decreased significantly (about 50 % drop). The test was repeated for eight samples and all the samples expressed the same behavior. It's important to point this degradation in ductility (thermal degradation) as it limits the practical temperature window at which SMP programing can take place. A summary of

the discussed properties is provided in Table 3 for all the considered deformation temperatures. Each reported value was obtained from averaging experimental results from two different samples at each deformation temperature. The yield strength is reported for samples tested below the glass transition, while alternatively the tensile strength is shown for the samples examined above the transition temperature which as discussed above exhibited linear response up to fracture.

Since full-field strain data was collected for the isothermal tensile tests, the EPON SMP's Poisson ratio at different temperatures was also extracted. By observing the local strain values in the region of interest (33x6 mm), the tensile deformation in the SMP proved to be homogeneous. Hence, the Poisson ratio was calculated by dividing the average compressive lateral strains (x-axis) with the tensile longitudinal strains (y-axis). Figure 54 shows the Poisson ratio calculated at different levels of deformation in the elastic region (time axis point increasing deformation levels) and for the different deformation temperatures. In general, the Poisson's ration increased with the increase in deformation temperature with an abrupt and sharp increase at deformations conducted in the soft phase ( $T_g > 130^\circ\text{C}$ ). At a high temperature of  $180^\circ\text{C}$ , thermal degradation was observed dropping the Poisson ratio to 0.478.

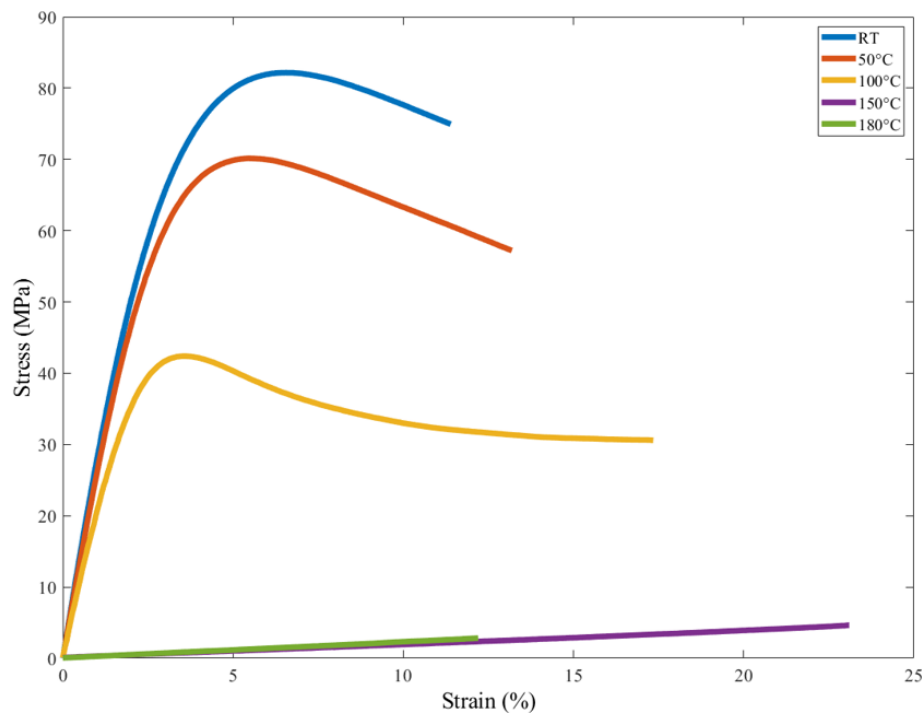


Figure 53: Tensile test of EPON SMP at different temperatures

Table 3: Tensile test summary

	E (Gpa)	Yield Strength (Mpa)	Yield Strain (%)	Fracture Strain (%)
RT	2.76	82.2	6.55	11.4
50°C	2.53	70.1	5.45	13.2
100°C	1.98	42.4	3.61	17.3
		Tensile Strength (MPa)		
150°C	0.019	4.64		23.1
180°C	0.023	2.83		12.2

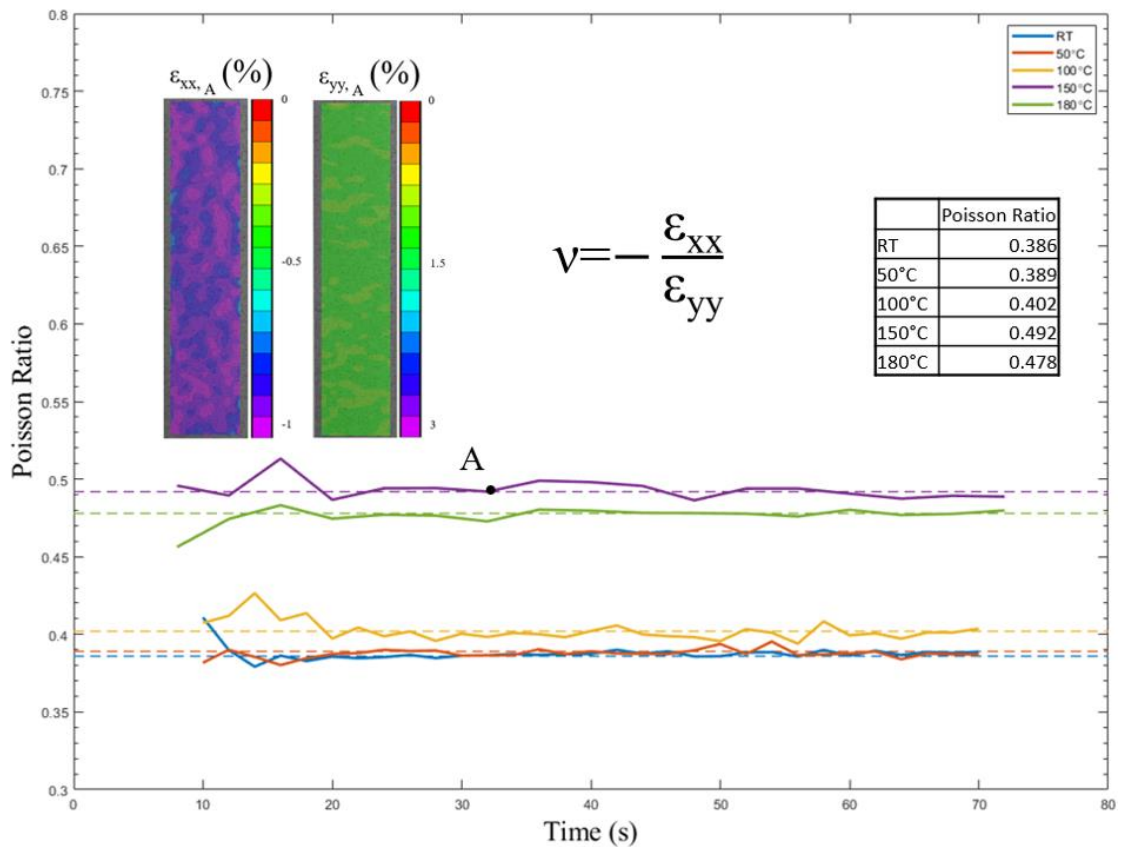


Figure 54: Poisson ratio at multiple temperatures

#### 4.4. Stress Relaxation

The stress relaxation experiments were conducted at different temperatures as discussed previously in section 3.4.3. The aim of this experiment was to provide insight on the stress relaxation phenomenon in the EPON polymer. As shown in Figure 55, the isothermal experiments at RT, 50°C, and 100°C all displayed a drop in the value of stress after being fixed in an axially deformed position. The drop in stress was observed

to be higher with the increase of temperature. Moreover, the samples experienced compressive stresses when returned to their initial positions. With time, the compressive stresses decreased in value but did not vanish. The residual stresses in the samples at the end of the experiments were compressive. This confirms the viscoelasticity of the EPON polymer. Figure 56 shows the normalized stress relaxation values after loading while Figure 57 shows the normalized stress relaxation values after the sample returns to its initial position.

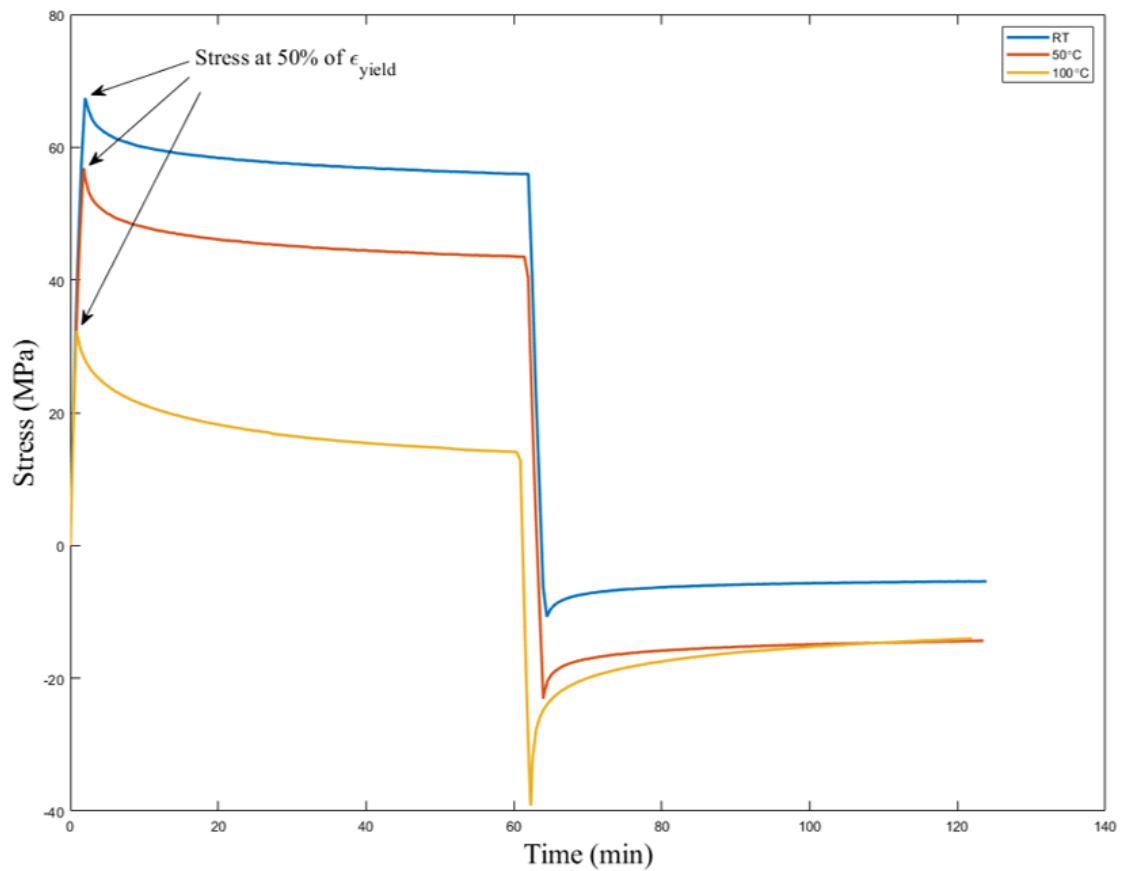


Figure 55: EPON SMP stress relaxation at different temperatures

#### 4.5. Stress-Free Tensile Recovery

The Tensile Recovery of the SMP was evaluated as mentioned previously in 3.4.4. Figure 58 shows representative stress-free thermal expansion data that was obtained from DIC images during the heating phase of the SMP prior to programming. It is observed that the thermal expansion coefficient ( $\alpha$ ) is the highest in the SMP's glass transition region ( $T_g \approx 130^\circ\text{C}$ ) having a value of  $6.6 \times 10^{-2} \text{ \%}/^\circ\text{C}$ . Moreover, the

thermal expansion coefficient in the SMP's hard phase ( $T < T_g$ ) is  $7.6 \times 10^{-3} \text{ \%/}^\circ\text{C}$  while being  $8.9 \times 10^{-3} \text{ \%/}^\circ\text{C}$  in the SMP's soft phase ( $T > T_g$ ). Furthermore, the total thermal strain induced in the SMP while heating from around  $25 \text{ }^\circ\text{C}$  to  $180^\circ\text{C}$  a significant is  $1.49 \text{ \%}$ . As will be discussed in subsequent sections, studying the EPON's thermal expansion was crucial for more accurate evaluation of the recovery stress for this high temperature SMP.

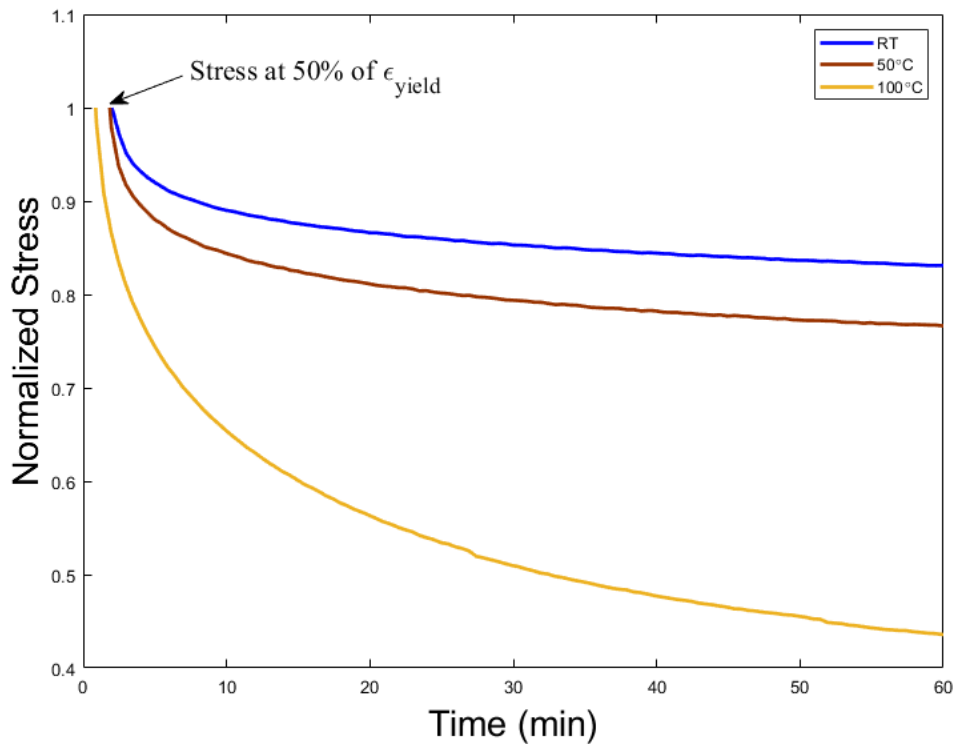


Figure 56: Normalized stress relaxation after loading

Following heating to  $180 \text{ }^\circ\text{C}$ , tensile samples were deformed in tension to  $6.3 \text{ \%}$  strain and subsequently cooled (i.e., programming as explained in section 3.4.4.). Figure 59 below shows the stress-free recovery of the programmed EPON SMP. The programmed sample was allowed to recover by placing it in a  $180^\circ\text{C}$  pre-heated oven. Thermal expansion was observed at the beginning of the experiment prior to recovery. The SMP recovered at a rate of  $0.13 \text{ \%/s}$  and the residual strain at the end of the experiment was  $1.65 \text{ \%}$ . Based on the data presented in Figure 58, the total amount of thermal strain in the sample is  $1.49 \text{ \%}$ . Therefore, the sample experienced  $97.6 \text{ \%}$  recovery with a non-recovered strain of  $0.16 \text{ \%}$ .

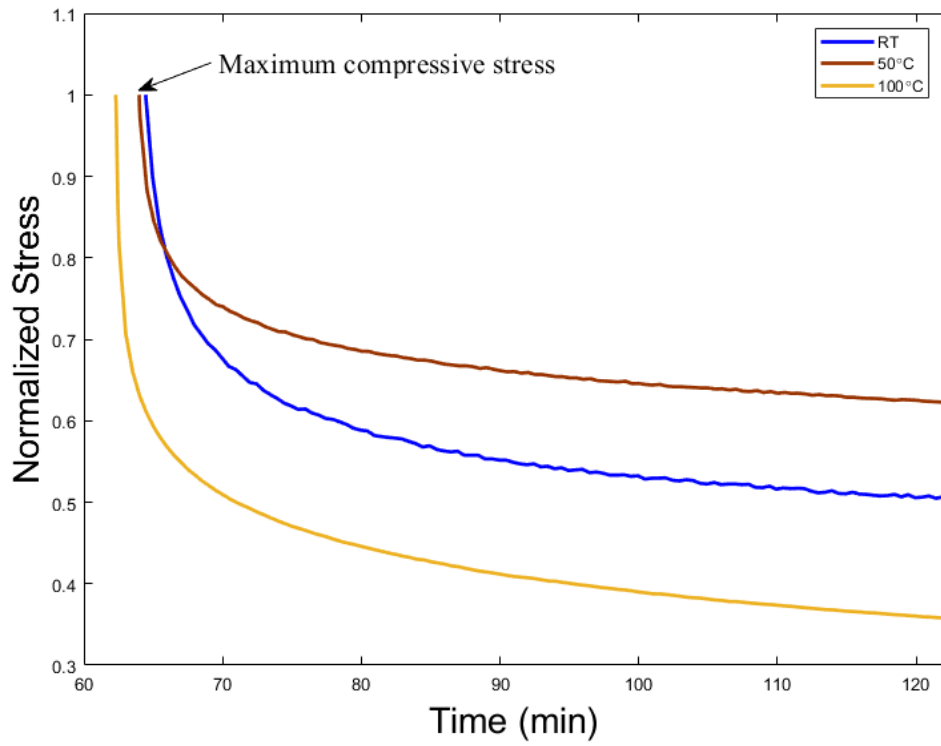


Figure 57: Normalized stress relaxation after returning to initial position

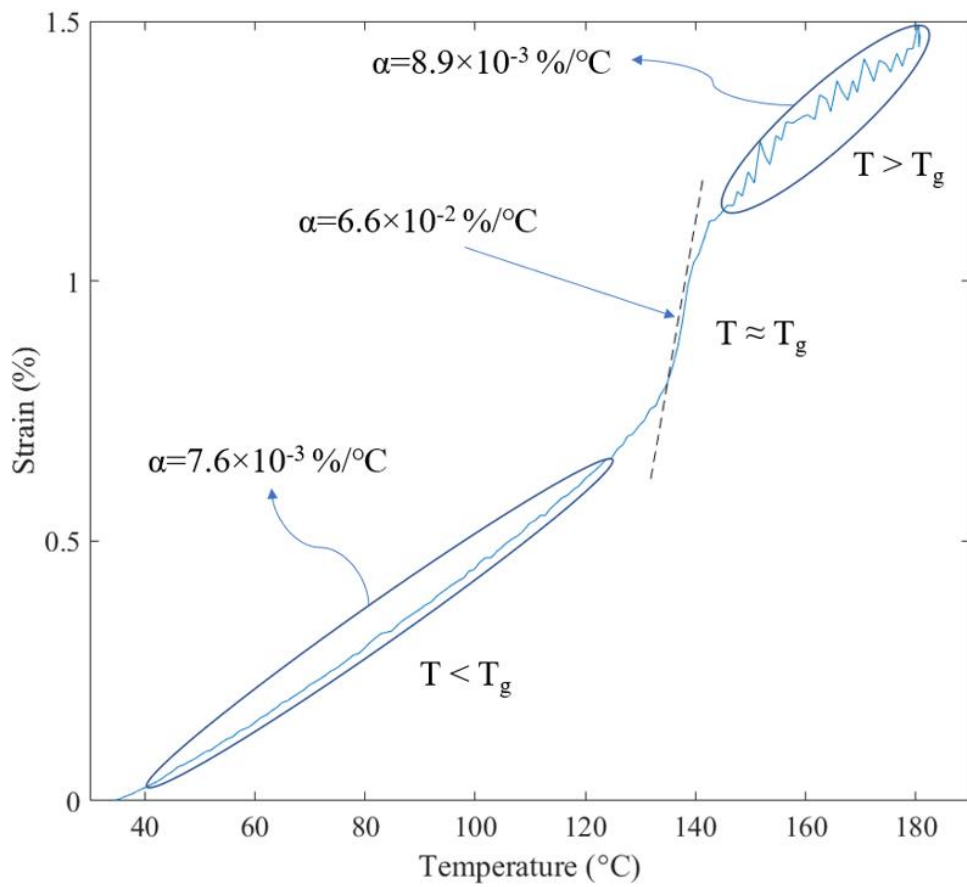


Figure 58: Stress-free thermal expansion

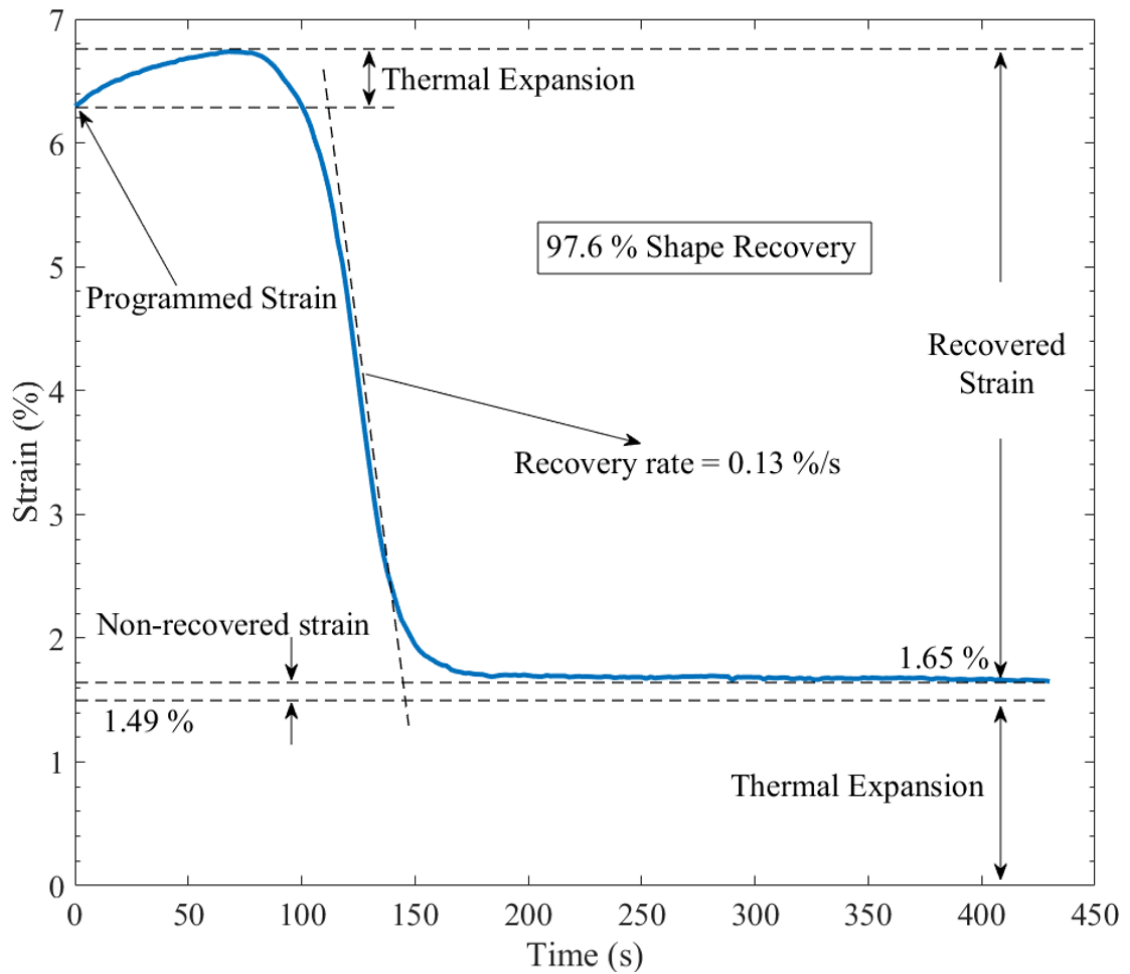


Figure 59: Stress-free tensile recovery

#### 4.6. Recovery Stress

The recovery stress of the SMP was measured as explained previously in 3.4.5. A programmed sample was heated to 180°C at a rate of 2°C/min while held tightly between the tensile grips of the UTM. The stress values were recorded and plotted against temperature as shown in Figure 60. The sample experienced around 18 MPa compressive stress due to thermal expansion and recovery was observed at the glass transition temperature ( $T_g \approx 125^\circ\text{C}$ ). The sample recovered to a tensile stress value of around 0.2 MPa hence, the recovery stresses were recorded around 18.2 MPa. After comparing with the literature, it was noticed that the recovery stress value of 18.2 MPa is very high. To prove and confirm this value, recovery at constant stress experiments were conducted as explained in section 3.4.6. and shown in section 4.7.

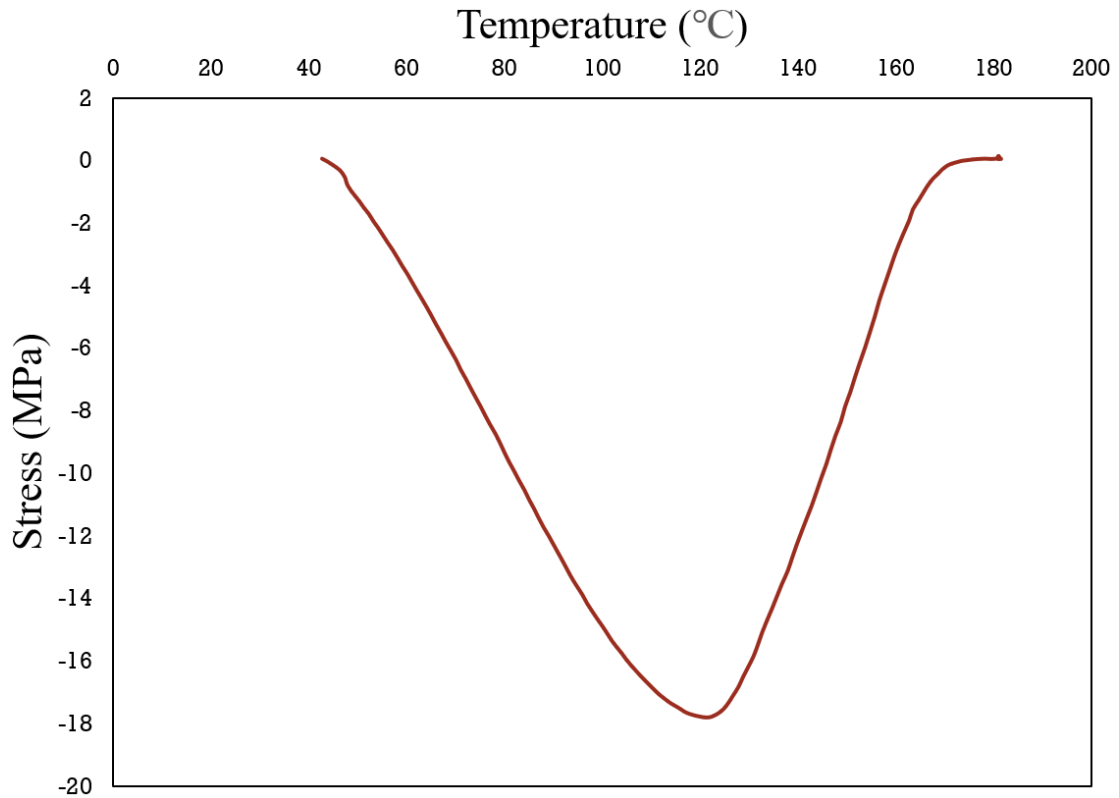


Figure 60: Recovery stress initial results

#### 4.7. Recovery at Constant Stress

Recovery experiments at constant stresses were conducted to verify the recovery stress results as explained previously in section 3.4.6. Programmed samples were heated to 180°C while holding a constant value of stress (*i.e.* 0.5MPa, 1MPa, 2MPa). At a constant stress value of 2 MPa, recovery was not observed as shown in Figure 61. It was concluded that the recovery stress value should be less than 2 MPa and the method used to obtain the value 18.2 MPa recorded in 4.6. needs to be modified. Recovery at constant stress was also conducted at a constant stress value of 0.5 MPa where recovery was observed hence, the recovery stress is higher than 0.5 MPa. The recovery process is shown in Figure 62. After removing the applied stress at the end of the experiment, residual strains were observed. The residual strains were therefore the thermal strains induced due to thermal expansion ( $\approx 1.49\%$ ) plus any non-recovered strain in the SMP ( $\approx 0.37\%$ ).

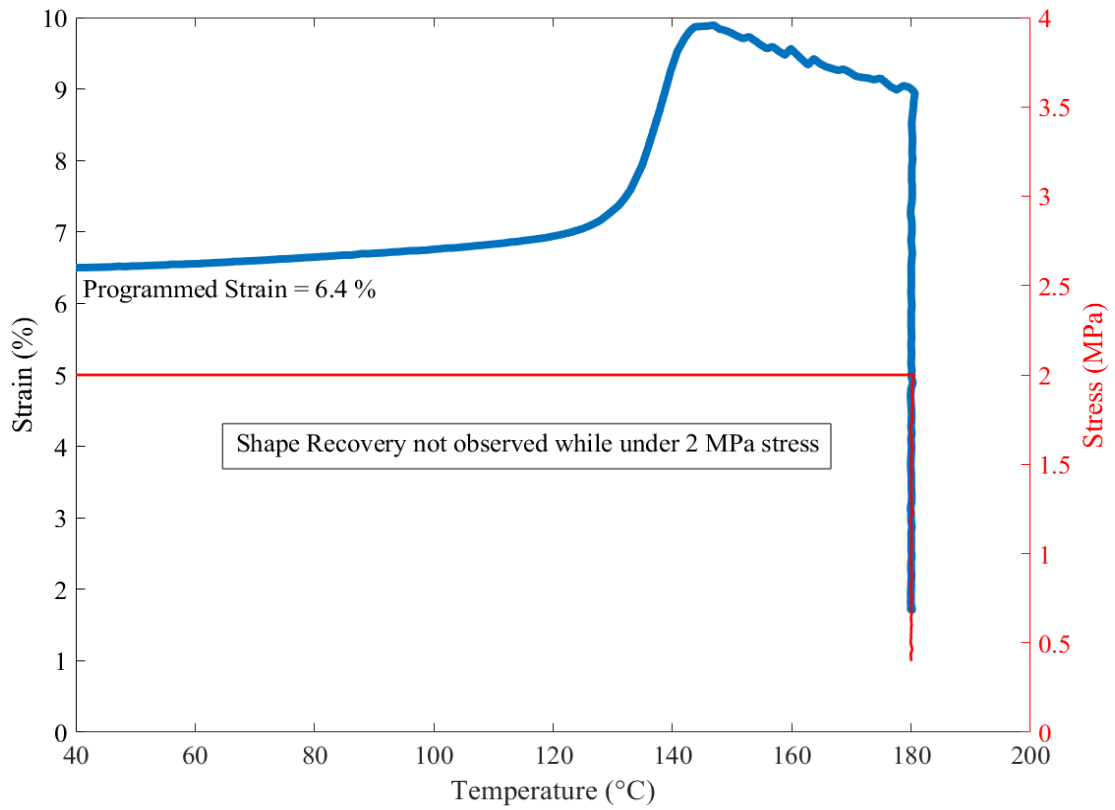


Figure 61: Recovery at constant stress 2 MPa

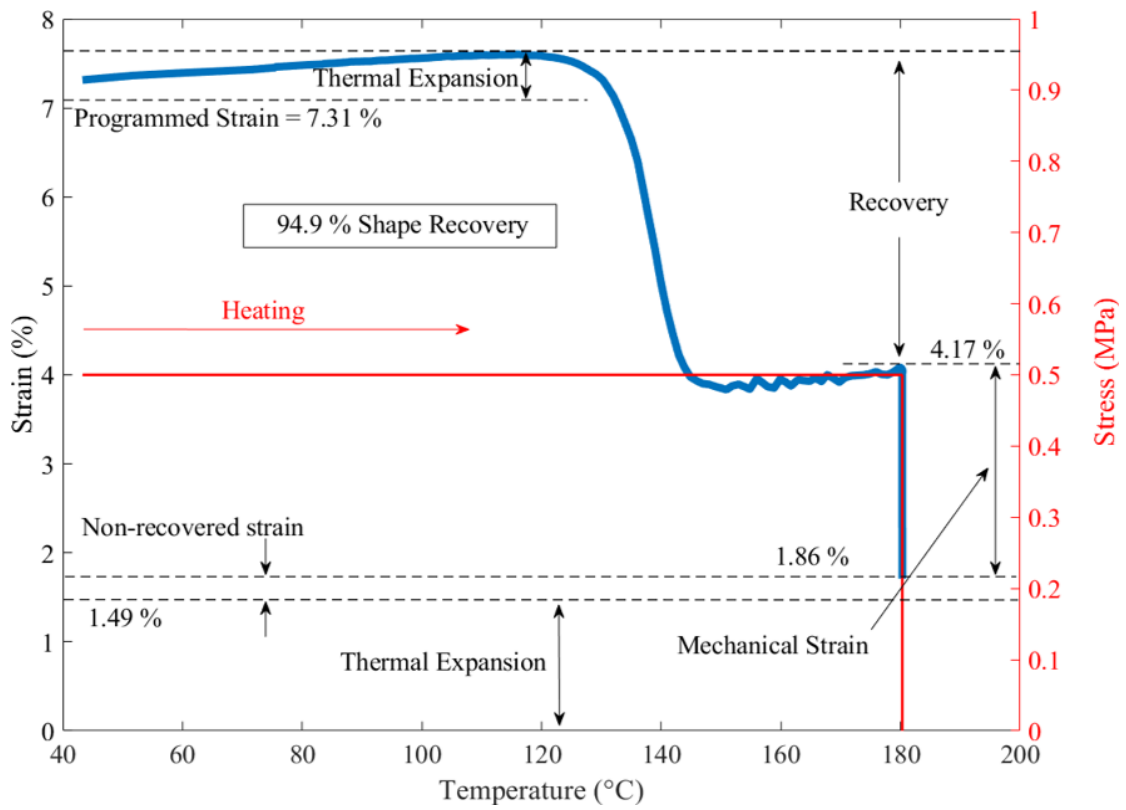


Figure 62: Recovery at constant stress 0.5 MPa

The recovery experiment at 1 MPa value of stress followed the same trend explained earlier and is shown in Figure 63. The recovered strain was significantly less than what is shown in Figure 62 due to the significantly higher mechanical strains (higher by a factor of  $\sim 2$ ). In addition, it is observed that the residual strains at the end of this experiment is higher than the measured value when the constant stress was 0.5MPa. It is deduced that the amount of non-recovered strains increases with the increase in the applied stress during the process of shape recovery. A summary of the programming and recovery strain magnitudes under constant applied stresses of 0.5 and 1.0 MPa is shown in Table 4.

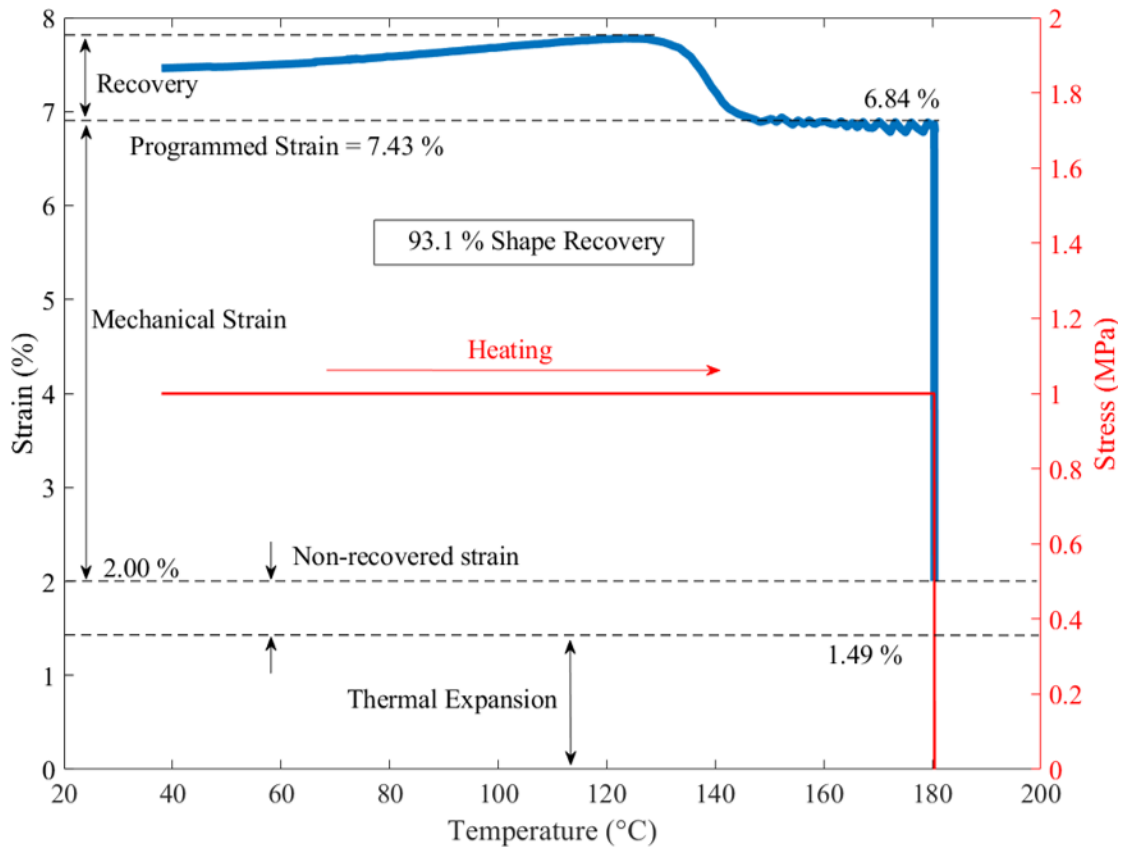


Figure 63: Recovery at constant stress 1 MPa

#### 4.8. Recovery Stress - Modified

The recovery stress method was modified as discussed previously and the results are shown in Figure 64, recovery started at around 115°C and ended at around 140°C providing 1.26 MPa recovery stress. It is important to note that due to the

viscoelastic properties of the SMP, some finite stress relaxation took place during recovery. This is clearly shown in Figure 64 between 140 and 180 °C. The SMP relaxed to a stress of around 1.1 MPa at 180°C.

Table 4: Recovery at constant stress summary

Stress (MPa)	Programming level (%)	Non-recovered strain (%)	% Shape Recovery
0.5	7.31	0.37	94.9
1	7.43	0.51	93.1

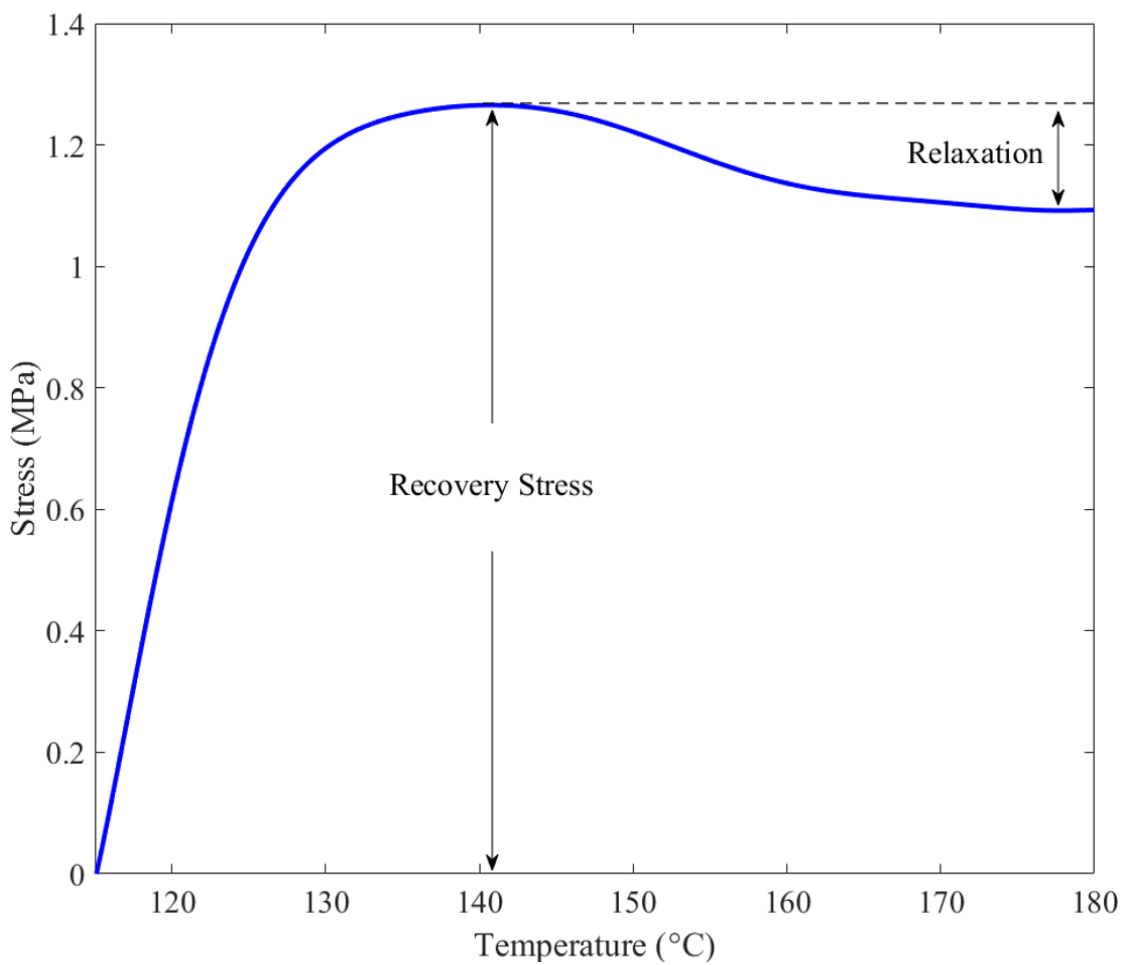


Figure 64: Recovery stress – modified

## Chapter 5. Conclusions and Recommendations

To conclude, the unique properties of SMPs continue to capture the interest of the aerospace industry. Driven by the interest to expand the range of potential use of SMPs in aerospace applications, a high temperature thermoset epoxy SMP ( $T_g \sim 130^\circ\text{C}$ ), named EPON SMP, was thoroughly investigated in this study. Throughout the literature, the focus has been on SMPs with low transformation temperatures below  $100^\circ\text{C}$ . Moreover, studies lack full-field characterization of the recovery properties of SMPs. This study provided comprehensive experimental analysis of the mechanical and shape memory properties of the aforementioned high temperature epoxy SMP. In addition, this study used full-field DIC analysis to provide further insight into the localization, heterogeneity and local recovery of shape memory strains. Furthermore, the study evaluated the recovery properties of SMPs at different loading conditions (*i.e.* bending and tensile) and proposed shape-recovery evaluation methods that can be later implemented on other SMPs. This research supports the following conclusions:

- SMP recovery is dependent on programmed strain and recovery temperature.
- Stress-free shape recovery observed for both uniformly and non-uniformly deformed shapes.
- Less shape recovery for the EPON SMP while under stress.
- Degradation in EPON SMP's ductility at elevated temperatures.
- The effects of thermal stresses and strains are highly significant in the EPON SMP programming and shape recovery processes. Hence, thermal expansion in EPON SMP should be given careful consideration while designing for an application.

Finally, the thorough investigation of the mechanical and shape recovery properties of the EPON SMP in this research leads to further recommendations and possible future work to advance in the shape memory polymers field. The recommendations and possible future work are as follows:

- To study the effect of varying the chemical composition of EPON SMP on its mechanical and shape recovery properties. This study is essential to obtain optimum properties for high temperature applications.
- To Fabricate a high temperature SMPC using EPON SMP as the matrix. Since the EPON SMP shows significant viscosity and long curing time, the

appropriate method for fabricating a fiber composite using it as a matrix requires further research and optimization.

- The lay-up technique is not recommended to fabricate EPON SMPCs. Few trials for fabricating EPON SMPCs using this technique were conducted in this study. However, and although shape memory properties were obtained, the programming window (*i.e.*, programming strains) was very small and limited by brittle fracture in the carbon fiber SMP composite. This aspect was mainly attributed to poor control of the carbon fiber-SMP volume fractions using the lay-up technique.
- To optimize EPON SMPC properties by varying the types of fibers used.
- To optimize EPON SMPC properties by varying the fiber to matrix ratio.
- All the aforementioned future investigations can aid in fabricating a practical self-deployable aerospace structure using SMPCs for the deployment actuation.

## References

- [1] H. Tobushi, H. Hara, E. Yamada, and S. Hayashi, “Thermomechanical properties of shape memory polymer of polyurethane series and their applications,” in *3rd International Conference on Intelligent Materials and 3rd European Conference on Smart Structures and Materials*, 1996, vol. 2779, pp. 418–424.
- [2] H. Tobushi, N. Ito, K. Takata, and S. Hayashi, “Thermomechanical constitutive modeling of polyurethane-series shape memory polymer,” in *Materials Science Forum*, 2000, vol. 327, pp. 343–346.
- [3] W. M. Sokolowski and S. C. Tan, “Advanced self-deployable structures for space applications,” *J. Spacecr. Rockets*, vol. 44, no. 4, pp. 750–754, 2007.
- [4] S. Dutton, D. Kelly, and A. Baker, *Composite Materials for Aircraft Structures*. American Institute of Aeronautics and Astronautics, 2004.
- [5] T. Williams, M. Meador, S. Miller, and D. Scheiman, “Effect of graphene addition on shape memory behavior of epoxy resins,” presented at the International SAMPE Technical Conference, Texas, United States, 2011.
- [6] D. M. Feldkamp and I. A. Rousseau, “Effect of the Deformation Temperature on the Shape-Memory Behavior of Epoxy Networks,” *Macromol. Mater. Eng.*, vol. 295, no. 8, pp. 726–734, 2010.
- [7] Y. Liu, C. Han, H. Tan, and X. Du, “Thermal, mechanical and shape memory properties of shape memory epoxy resin,” *Mater. Sci. Eng. A*, vol. 527, no. 10–11, pp. 2510–2514, 2010.
- [8] H. Meng and G. Li, “A review of stimuli-responsive shape memory polymer composites,” *Polymer*, vol. 54, no. 9, pp. 2199–2221, 2013.
- [9] Z. Wang and Z. C. Kang, *Functional and Smart Materials: Structural Evolution and Structure Analysis*. Springer Science & Business Media, 2012.
- [10] T. Xie, “Recent advances in polymer shape memory,” *Polymer*, vol. 52, no. 22, pp. 4985–5000, 2011.
- [11] K. Gall, M. L. Dunn, Y. Liu, D. Finch, M. Lake, and N. A. Munshi, “Shape memory polymer nanocomposites,” *Acta Mater.*, vol. 50, no. 20, pp. 5115–5126, 2002.

- [12] H.-Y. Jiang and A. M. Schmidt, “The structural variety of shape-memory polymers,” *Shape-Memory Polym. Multifunct. Compos. CRC Press. Boca Rat.*, pp. 21–63, 2010.
- [13] J. Hu, *Shape Memory Polymers and Textiles*. Elsevier, 2007.
- [14] J. Leng, X. Lan, Y. Liu, and S. Du, “Shape-memory polymers and their composites: stimulus methods and applications,” *Prog. Mater. Sci.*, vol. 56, no. 7, pp. 1077–1135, 2011.
- [15] K. Hearon *et al.*, “Porous shape-memory polymers,” *Polym. Rev.*, vol. 53, no. 1, pp. 41–75, 2013.
- [16] A. Adler, L. Davis, D. Cohen, J. Winter, G. Spanjers, S. Easley, G. Ginet, and B. Dichter, “Deployable structures space science experiment for large aperture, high power missions in MEO,” in *45th AIAA/ASME/ASCE/AHS/ASC Structures, Structural Dynamics & Materials Conference*, 2004, p. 1571.
- [17] E. Hornbogen, “Comparison of shape memory metals and polymers,” *Adv. Eng. Mater.*, vol. 8, no. 1–2, pp. 101–106, 2006.
- [18] W. Voit, T. Ware, R. R. Dasari, P. Smith, L. Danz, D. Simon, S. Barlow, S. R. Marder, K. Gall, “High-strain shape-memory polymers,” *Adv. Funct. Mater.*, vol. 20, no. 1, pp. 162–171, 2010.
- [19] W. Francis, M. S. Lake, K. Mallick, G. E. Freebury, and A. Maji, “Development and testing of a hinge/actuator incorporating elastic memory composites,” in *44th AIAA Structures, Structural Dynamics, and Materials Conference*, 2003, pp. 7–10.
- [20] X. Lan, R. Zhang, Y. Liu, J. Leng, “Fiber reinforced shape-memory polymer composite and its application in a deployable hinge,” in *52nd AIAA/ASME/ASCE/AHS/ASC Structures, Structural Dynamics and Materials Conference*, 2011, pp. 2115-2124.
- [21] P. Keller *et al.*, “Development of a deployable boom for microsatellites using elastic memory composite material,” in *45th AIAA/ASME/ASCE/AHS/ASC Structures, Structural Dynamics & Materials Conference*, 2004, pp. 1603-1611.
- [22] S. C. Arzberger *et al.*, “Elastic memory composites (EMC) for deployable industrial and commercial applications,” in *Smart Structures and Materials 2005: Industrial and Commercial Applications of Smart Structures Technologies*, 2005, vol. 5762, pp. 35–48.

- [23] D. Campbell, M. Lake, M. Scherbarth, E. Nelson, and R. Six, “Elastic memory composite material: an enabling technology for future furlable space structures,” in *46th AIAA/ASME/ASCE/AHS/ASC Structures, Structural Dynamics and Materials Conference*, 2005, pp. 2362-2370.
- [24] C. Hazelton, K. Gall, E. Abrahamson, M. Lake, and R. Denis, “Development of a prototype elastic memory composite STEM for large space structures,” in *44th AIAA/ASME/ASCE/AHS/ASC Structures, Structural Dynamics, and Materials Conference*, 2003, pp. 1977-1986.
- [25] R. Barrett, R. Taylor, P. Keller, M. Lake, T. Stern, G. Freebury, N. Beidleman, “Design of a solar array to meet the standard bus specification for operation responsive space,” in *48th AIAA/ASME/ASCE/AHS/ASC Structures, Structural Dynamics, and Materials Conference*, 2007, pp. 2332-2342.
- [26] M. Schultz, W. Francis, D. Campbell, and M. Lake, “Analysis techniques for shape-memory composite structures,” in *48th AIAA/ASME/ASCE/AHS/ASC Structures, Structural Dynamics, and Materials Conference*, 2007, pp. 2401-2411.
- [27] R. Barrett, R. Taylor, P. Keller, D. Codell, and L. Adams, “Deployable reflectors for small satellites,” presented at the 21th Annual Conference on Small Satellites, Utah, United States, 2007.
- [28] P. Keller, M. Lake, D. Codell, R. Barrett, R. Taylor, and M. Schultz, “Development of elastic memory composite stiffeners for a flexible precision reflector,” in *47th AIAA/ASME/ASCE/AHS/ASC Structures, Structural Dynamics, and Materials Conference 14th AIAA/ASME/AHS Adaptive Structures Conference 7th*, 2006, pp. 2179-2189.
- [29] Miller-Stephenson Chemicals. “Why Everyone Chooses EPON™ & EPIKURE™ Epoxy Resins,” Internet: <https://miller-stephenson.com/choose-epon-epikure-epoxy-resins/>, November 14, 2017 [April, 2019].
- [30] W. Abuzaid, H. Sehitoglu, and J. Lambros, “Plastic strain localization and fatigue micro-crack formation in Hastelloy X,” *Mater. Sci. Eng. A*, vol. 561, pp. 507–519, 2013.
- [31] F. L. Ji and J. L. Hu, “Comparison of shape memory polyurethanes and polyurethane-ureas having crystalline reversible phase,” *High Perform. Polym.*, vol. 23, no. 4, pp. 314–325, 2011.

- [32] J. Ivens, M. Urbanus, and C. De Smet, "Shape recovery in a thermoset shape memory polymer and its fabric-reinforced composites.," *Express Polym. Lett.*, vol. 5, no. 3, 2011.
- [33] M. Simonsen, 'Strain Tensors and Criteria in Vic', Internet: <http://www.correlatedsolutions.com/support/index.php?/Knowledgebase/Article/View/2/0/strain-tensors-and-criteria-in-vic>, July 18, 2017 [November 2017]
- [34] B. McGinty, 'Principal Stresses & Strains', Internet: <http://www.continuummechanics.org/principalstressesandstrains.html>, December 4, 2016 [October 2017].

## **Vita**

Mohamad Youssef ElMaoud was born in 1994, in Abu Dhabi, United Arab Emirates. He received his primary and secondary education in AlNahda National Schools, Abu Dhabi, UAE. He received his B.Sc. degree in Mechanical Engineering with a minor in Engineering Management from the American University of Sharjah in 2015. From 2013 to 2015, he worked as a part time Manufacturing Lab Assistant in the American University of Sharjah.

In September 2015, he joined the Mechanical Engineering master's program in the American University of Sharjah. He became a Graduate Teaching Assistant at the American University of Sharjah in 2016. Since January 2017, Mohamad ElMaoud became a full-time Laboratory Engineer and Teaching Assistant at Abu Dhabi Polytechnic Institute, Abu Dhabi, UAE. In March 2018, he received “Best Paper Award” in the UAE Graduate Student Research Conference 2018.